Received: 23 November 2020 | Accepted: 4 December 2020

DOI: 10.1111/bre.12538

RESEARCH ARTICLE

Basin Research IAS EAGE WILEY

Syn-rift sediment gravity flow deposition on a Late Jurassic fault-terraced slope, northern North Sea

Fabian Tillmans[1] | **Robert L. Gawthorpe**[1] | **Christopher A.-L. Jackson**[2] | **Atle Rotevatn**[1]

[1]Department of Earth Science, University of Bergen, Bergen, Norway

[2]Basins Research Group (BRG), Department of Earth Science & Engineering, Imperial College, London, UK

Correspondence
Fabian Tillmans, Department of Earth Science, University of Bergen, PO Box 7800, 5020 Bergen, Norway.
Email: fabian.tillmans@gmail.com

Funding information
Research Council of Norway, Grant/Award Number: 255229; Aker BP; ConocoPhillips; DNO; Equinor; Neptune; Tullow Oil

Abstract

Structurally controlled bathymetry in rifts has a significant influence on sediment routing pathways and depositional architecture of sediment gravity flow deposits. In contrast to rift segments characterized by crustal-scale half-grabens, the tectono-stratigraphic evolution of deep-water rift domains characterised by distributed faulting on narrow fault terraces has received little attention. We use 3D broadband seismic data, calibrated by boreholes, from the Lomre and Uer terraces in the northern North Sea rift to investigate Late Jurassic syn-rift sediment gravity flow systems on fault-terraced slopes. The sediment gravity flow fairways were sourced from hinterland drainages via basin margin deltaic systems on the Horda Platform to the southeast. The deep-water sedimentary systems evolve from initial, widespread submarine channelized lobe complexes, through submarine channels, to incised submarine canyons. This progressive confinement of the sediment gravity flow system was concomitant with progressive localization of strain onto the main terrace-bounding faults. Although the normal fault network on the terraces has local impact on deep-water sediment transport and the architecture of gravity flow deposits, it is the regional basin margin to rift axis gradient that dominantly controls deep-water sediment routing. Furthermore, the gravity flow deposits on the Lomre and Uer terraces were predominantly sourced by rift margin deltaic systems, not from erosion of local uplifted footwall crests, emphasising the significance of hinterland catchments in the development of volumetrically significant deep-water syn-rift depositional systems.

KEYWORDS

gravity flows, normal fault terraces, rift basins, seismic geomorphology, submarine channels and canyons, submarine lobes, syn-rift sequences, turbidites

1 | INTRODUCTION

The stratigraphic evolution of rift basins is closely linked to growing normal faults that control most of the surface topography during rifting (Cowie et al., 2005; Gawthorpe & Leeder, 2000). The way in which fault segments grow and link to form through-going fault arrays is recognized as a first-order control on syn-rift accommodation space, sediment supply and sediment routing (Anders & Schlische, 1994; Cowie et al., 2000, 2005; Gawthorpe &

Leeder, 2000; Prosser, 1993). Existing studies suggest that early-stage rift basins, often referred to as 'rift initiation stage' (Jackson et al., 2006; Prosser, 1993; Ravnås & Steel, 1998), are dominantly fill-to-spill basins characterized by terrestrial to shallow marine depositional systems. As rifting progresses, localization of faulting onto few, large normal faults leads to increasing subsidence rates and accommodation creation often significantly outpacing sediment supply in the rift climax stage, which results in deep-water sediment-starved rift basins (Gawthorpe et al., 1994; Gawthorpe & Leeder, 2000; Prosser, 1993; Ravnås & Steel, 1998). Most tectono-sedimentary studies of rift basins focus on major, crustal-scale tilted fault blocks. Yet, significant differences in erosion, sediment transport and deposition are expected to occur in areas characterized by structurally complex, narrow fault terraces that often characterize rift accommodation zones (Duffy, Brocklehurst, et al., 2015; Færseth & Ravnås, 1998; Jackson & Leeder, 1994; Younes & McClay, 2002).

Deep-water deposits in active rifts are usually depicted as fault-scarp aprons along major basin margin faults and as submarine gravity flow fans that are either fed through relay zones or sourced locally from uplifted footwalls (Leeder & Gawthorpe, 1987; Prosser, 1993; Ravnås & Steel, 1998). These settings are frequently documented on subsurface- and outcrop data around the world, for example, in the Gulf of Suez (Leppard & Gawthorpe, 2006), East Greenland (Henstra et al., 2016), the Tamtsag Basin (Jia et al., 2014) and Lake Baikal (Nelson et al., 1999). Studies from the Late Jurassic of the northern North Sea have documented such systems, for example, in the Brae submarine fan system (Fraser et al., 2003; Turner et al., 2018). Important turbidite systems are also observed on the hanging wall dipslope of large rotated fault blocks (Jackson et al., 2011; Nøttvedt et al., 2000; Ravnås & Steel, 1997). In general, it is further recognized that deep-water axial sediment routing can evolve from these short transverse sedimentary fairways and transport coarse-grained sediments along the rift axis (Gawthorpe & Leeder, 2000; Prosser, 1993; Ravnås & Steel, 1998).

We utilized new regional high-resolution 3D broadband seismic reflection data, calibrated by a comprehensive well database, to investigate the Late Jurassic evolution of deep-water sedimentary systems on the Lomre and Uer terraces, northern North Sea (Figure 1). Our objectives are to (i) illustrate the evolution of syn-rift deep-water depositional systems downdip of major basin-margin deltaic systems, (ii) investigate the interaction of these systems with the complex normal fault terrace topography and (iii) identify the impact of fault geometry on associated deep-water depocenters. The study advances current tectono-sedimentary models of deep-water depositional systems in rifts, which are mostly focused on local footwall-sourced, transverse depositional systems in major crustal-scale half graben.

Highlights

- Integration of well data, seismic stratigraphy and 3D seismic geomorphology to elucidate on the regional evolution of deep-water syn-rift depositional systems on closely spaced fault terraces
- Evolution of a deep-water syn-rift clastic system, which can be linked from shallow-marine source to sink
- Rift margin sediment supply with hinterland drainage is main source for sediments to the syn-rift gravity flow fairways
- Deep-water sediment routing on fault terraces is dominantly controlled by the regional slope gradient rather than the local fault-block topography associated with tilting and crestal uplift
- Updated conceptual models for deep-water sediment routing and depositional architecture in syn-rift settings with dominantly distributed strain

2 | REGIONAL GEOLOGICAL SETTING

The greater Viking Graben area is located in the northern North Sea and developed as a result of two distinct phases of rifting, one in the Permo-Triassic and the second in the Late Jurassic to Early Cretaceous (Badley et al., 1988; Færseth, 1996; Odinsen et al., 2000; Zanella et al., 2003) (Figure 1). In the Late Jurassic, the study area comprised marginal platform areas, deep rift-axis grabens and intervening normal faulted terraces that created a stepped slope profile. Recent studies using 3D seismic reflection and well data have constrained the structural framework (Duffy, Bell, et al., 2015; Phillips et al., 2019; Reeve et al., 2015; Whipp et al., 2014) and sedimentological evolution (Dreyer et al., 2005; Holgate et al., 2013, 2015; Patruno et al., 2015; Stewart et al., 1995) of associated shallow marine deposits. However, little attention has been given to the adjacent terrace areas and their Late Jurassic deep-water, syn-rift sedimentology.

The majority of the up to 3 km thick, Late Jurassic syn-rift strata in the rift-axis graben is characterized by basinal, shale-rich units of the Heather and Draupne Formations (Fraser et al., 2003; Vollset & Doré, 1984). The transition from Heather Formation mudstone to Draupne Formation black shale deposition marks a time transgressive surface, younging towards the basin margin and on intrabasinal highs, but is approximately of late Oxfordian to late Kimmeridgian age (Fraser et al., 2003; Vollset & Doré, 1984). The shift to

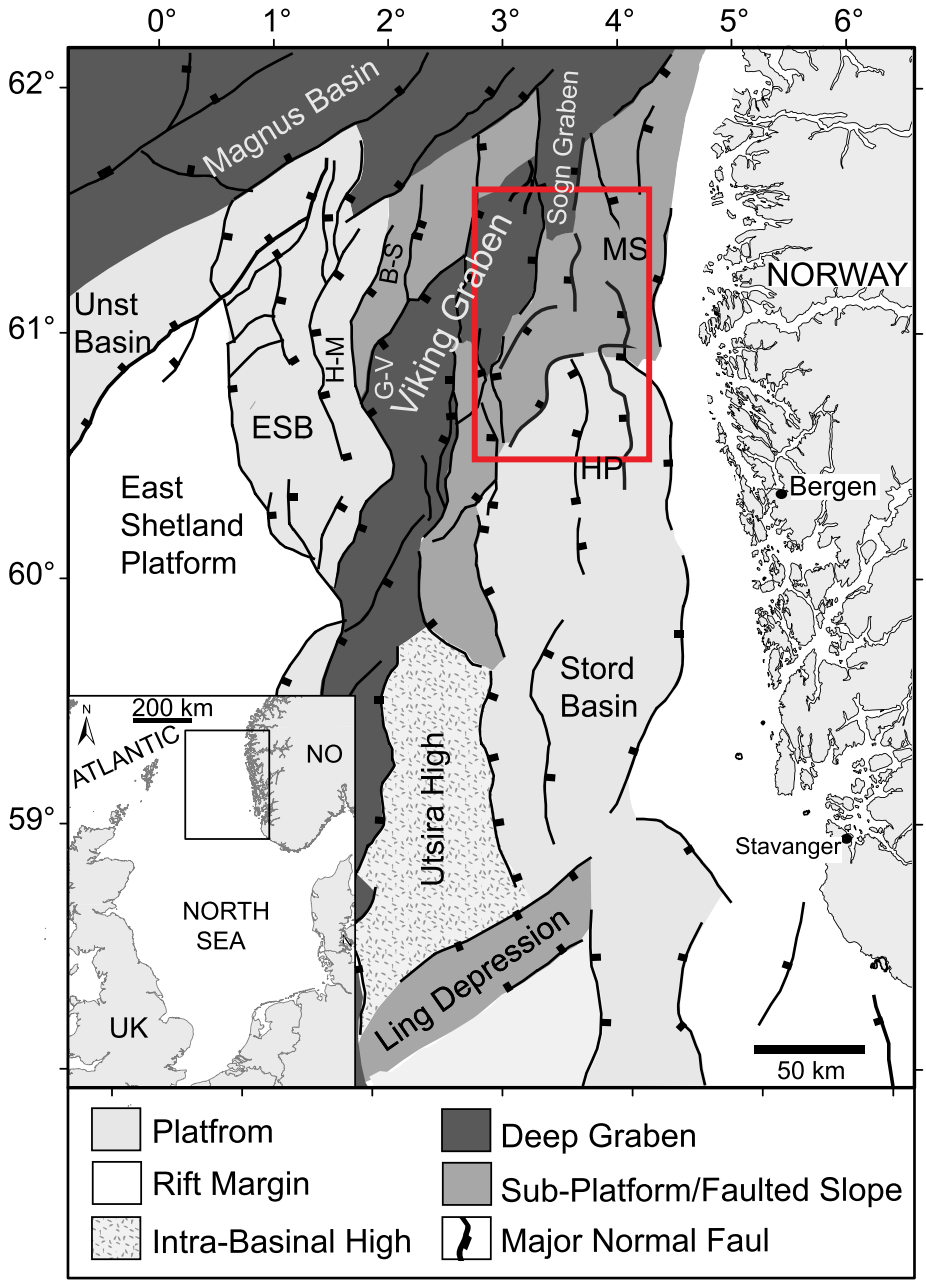

FIGURE 1 Structural overview map of the northern North Sea basin system (from Bell et al. (2014) after Færseth (1996)). Red rectangle marks the outline of Figure 2. ESB = East Shetland Basin, B-S = Brent-Statfjord Fault, G-V = Gullfaks-Visund Fault, MS = Måløy Slope, HP = Horda Platform

deposition of the highly radioactive Draupne Formation shale has been linked to peak extension and associated basin deepening (e.g. Færseth & Ravnås, 1998).

Contemporaneous shallow marine and deltaic sequences, sourced from major hinterland catchments on the Norwegian mainland, are developed across the Horda Platform on the eastern margin of the Viking Graben (Figures 2 and 3) (Fraser et al., 2003; Holgate et al., 2013; Patruno et al., 2015; Ravnås & Bondevik, 1997). Periodic outbuilding of these shallow marine and deltaic systems created the Krossfjord (Bathonian), Fensfjord (Callovian) and Sognefjord formations (Oxfordian to Kimmeridgian) (Holgate et al., 2013; Patruno et al., 2015; Ravnås & Bondevik, 1997) (Figure 2a). These basin margin depositional systems supplied sediment to deep-water gravity flow systems across faulted terraces towards rift axis grabens. The resulting gravity flow deposits are informally referred to as intra-Heather- and intra-Draupne Formation sandstones (Koch et al., 2017; Ravnås et al., 2000; Zhong et al., 2020) (Figure 2b). Large-scale Late Jurassic canyon incision (ca. Kimmeridgian – early Tithonian) has been described along the eastern margin of the North Viking- and Sogn grabens, including the Lomre and Uer Terraces (Jackson et al., 2008; Koch et al., 2017; Sømme et al., 2013).

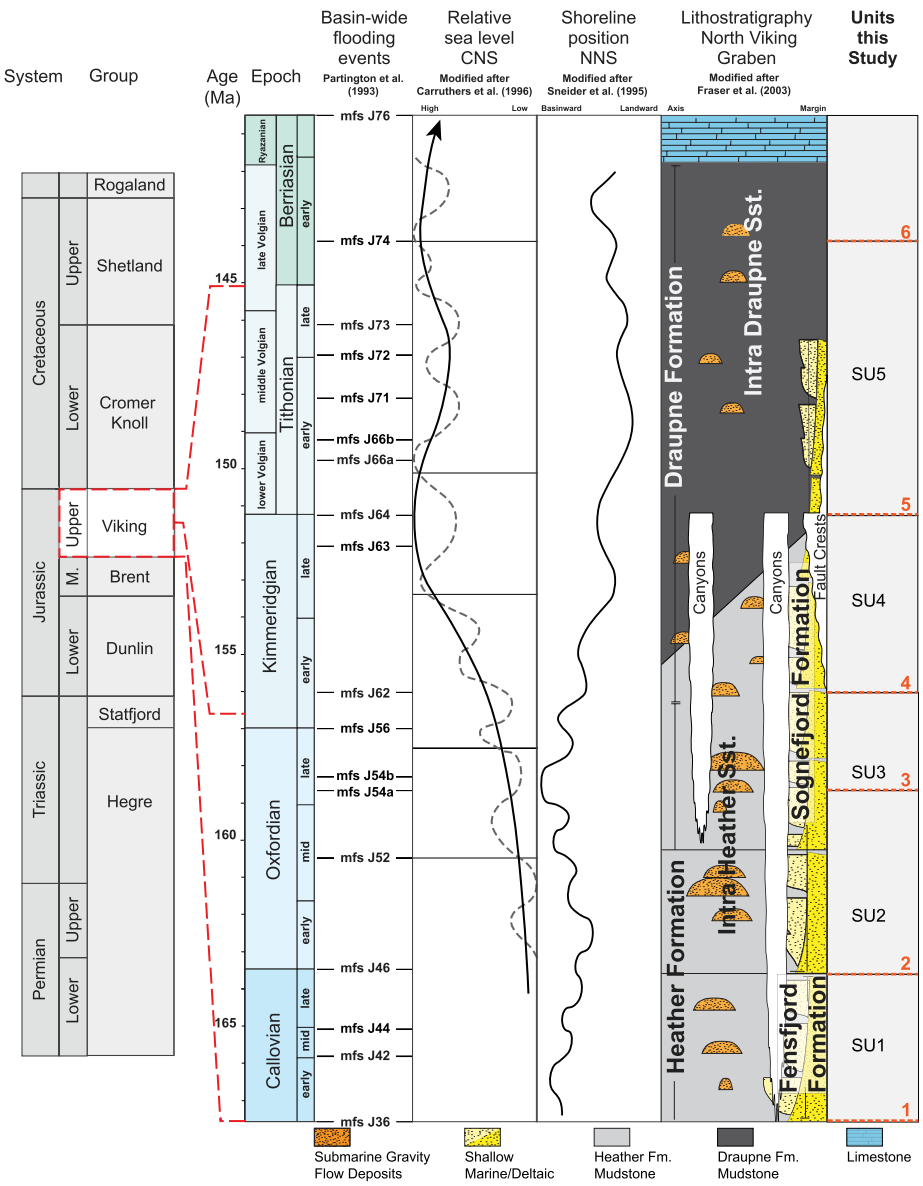

FIGURE 2 Chronostratigraphic table of the Late Jurassic, modified after Fraser et al. (2003). Right column shows stratigraphic subdivision in this study. Dashed orange line depicts approximate chronostratigraphic position of mapped seismic surfaces, SU = Seismic Unit

3 | DATA AND METHODS

Our study uses new 3D broadband seismic reflection data of the Northern North Sea covering ca. 9,000 km^2 from the eastern flank of the North Viking Graben (Figures 1 and 3). The version used in this study is post-stack depth migrated and time-stretched, meaning that vertical values here refer to depth in two-way time (TWT). The seismic data have an inline spacing of 18.75 m and crossline spacing of 12.5 m, and processed in zero phase with SEG normal polarity convention, where a downward increase in acoustic impedance results in a peak response (blue reflection).

The seismic resolution in the Late Jurassic of the Lomre and Uer terraces is ca. 15 m vertical and 30 m lateral based on a maximum frequency of about 62 Hz at −20 dB and an average interval velocity of 3,359 m/s (Figure 4). Due to the relatively deep burial of the Late Jurassic sedimentary systems (ca. 2.5–3.5 s (TWT)) on the Lomre and Uer terraces, the impedance contrasts between sandstones and mudstones are reduced compared to shallower strata (Cook & Sawyer, 2015). Thus, imaging depositional shapes and geometries is relatively challenging, and integration of well data and advanced seismic attributes are essential parts of analysing the depositional systems.

We used core, mud log and well log data from 40 exploration wells to integrate sedimentological calibration of the seismic geomorphology. Figure 4 shows the location of the exploration wells that were used in order to constrain ages,

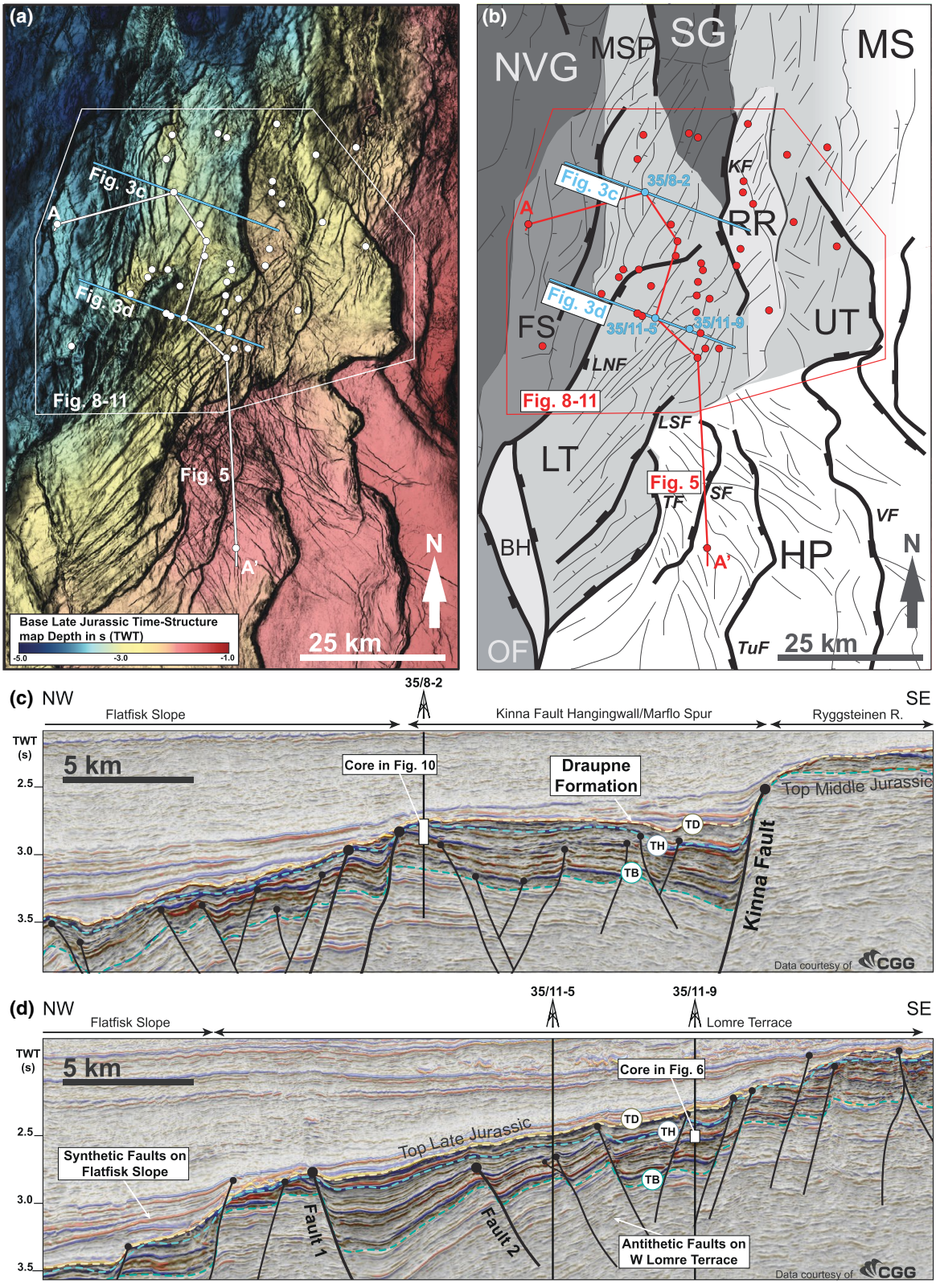

FIGURE 3 Base Late Jurassic syn-rift seismic surface of the eastern flank of the North Viking Graben (location in Figure 1), polygon marks outline of study area, circles are well locations used in this work. (a) Time-structure map of the Top of the Middle Jurassic BRENT Group with variance attribute overlay. (b) Simplified map illustrating the subdivision into structural elements: HP = Horda Platform, LT = Lomre Terrace, UT = Uer Terrace, FS = Flatfisk Slope, NVG = North Viking Graben, MSP = Marflo Spur, RR = Ryggsteinen Ridge, MS = Måløy Slope, SG = Sogn Graben, BH = Brage Horst, OF = Oseberg Fault Block Major Faults are KF = Kinna Fault, TF = Troll Fault, SF = Svarte Fault, TuF = Tusse Fault, VF = Vette Fault, LSF = Lomre South Fault, LNF = Lomre North Fault (in this study also 'Fault 3'). (c) Cross section through hanging wall of Kinna Fault, location in Figure 3a/b and annotation from Figure 5. (d) Cross section through the northern Lomre Terrace, location in Figure 3a/b and annotation from Figure 5

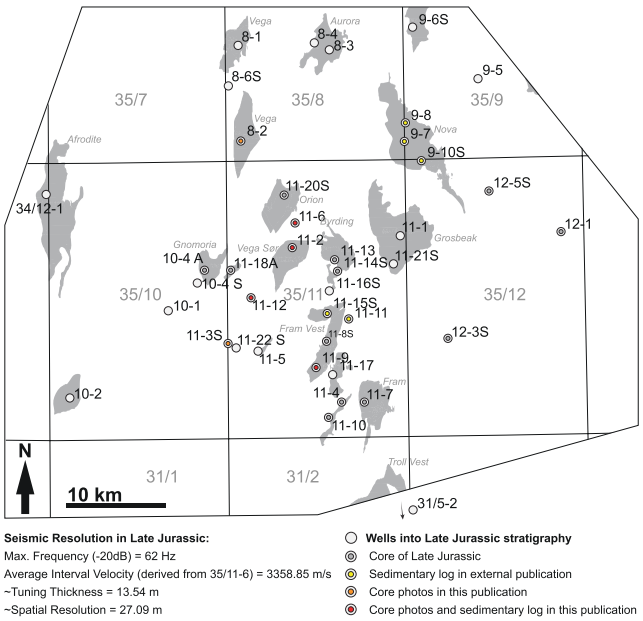

FIGURE 4 Map showing the location of the exploration wells used in this study (for location of 31/5-2 see Figure 3). Maximum seismic frequency (−20 dB) averaged over thickest Late Jurassic stratigraphy of the study area located in the hanging wall of the Kinna Fault. Average interval velocity from adjacent well 35/11-6

lithology and depositional environment of the Late Jurassic stratigraphy. We used raw and interpreted well data from the Norwegian Petroleum Directorate (NPD) data repository and company-internal biostratigraphic reports. The majority of these wells are located in crestal locations, which undersamples syn-rift strata in hanging walls and hanging wall dip slopes.

Frequency decomposition of the seismic data was used to visualize subtle depositional elements of varying stratigraphic thickness that, otherwise, can be masked in standard attribute maps (Koson et al., 2014; Laughlin et al., 2003; McArdle & Ackers, 2012; Partyka et al., 1999). We used a combination of frequency decomposition red-green-blue (RGB) colour blending and the exchroma SRGB method, which co-renders image-processed seismic attribute cubes into RGB colour blends (Laake, 2015). The three exchroma attribute cubes are generated by calculating root-mean-square (RMS) amplitude values over narrow windows of different averaging window sizes for each attribute cube (red channel = longest RMS window, green channel = mid-sized RMS window, blue channel = shortest RMS window). This method extracts very subtle heterogeneities within the seismic data and especially aids the interpretation in areas of low impedance contrast.

We combine the variance attribute (Chopra & Marfurt, 2007) with RGB blends in a multi-attribute displays to illustrate vertical, as well as lateral heterogeneity and, thus, maximize the seismic geomorphologic signature of the deep-water sedimentary systems. The RGB blends extract attribute values from within the mapped seismic units over defined vertical windows, typically between 1 and 15 ms (TWT), depending on stratigraphic thickness and clearest seismic geomorphologic signature. The interpretation of these attribute maps is further supported by time-thickness maps of individual stratigraphic units. These maps reveal the large-scale spatial and temporal evolution of thickness patterns, which allow for interpretation of structural and sedimentological controls on thickness variations within the syn-rift depocenters.

4 | STRUCTURAL ELEMENTS

Figure 3 shows a blended variance time-structure map of the base syn-rift Horizon 1, which broadly coincides with the top of the Brent Group throughout most of the eastern flank of the Northern Viking Graben. The North Viking Graben is part of a larger, right-stepping rift axis formed by 30–50 km wide and 70–100 km long graben segments (e.g. Færseth et al., 1998). Its eastern margin is defined by the northernmost part of a 300 km long, N-S-trending structural high, referred to as Horda Platform (e.g. Badley et al., 1988; Bartholomew et al., 1993; Glennie, 1990) (Figure 3). The Måløy Slope marks the eastern rift margin to the N of the Horda Platform and forms the eastern margin of the Sogn Graben, the northernmost graben segment of the Late Jurassic northern North Sea rift system (e.g. Bell et al., 2014; Færseth et al., 1998). The North Viking Graben is asymmetric and bound by a crustal-scale border fault to the W (Fossen et al., 2010), and down-stepping tectonic terraces to the E (Ravnås et al., 2000). Important structural elements between marginal Horda Platform and the deep North Viking Graben are the Lomre and Uer terraces, two intra-basinal highs (Ryggsteinen Ridge and Marflo Spur) and the Flatfisk Slope (Figure 3).

4.1 | Horda Platform/Måløy Slope

The Horda Platform forms a regional palaeogeographical high during the Late Jurassic (Duffy, Bell, et al., 2015; Whipp et al., 2014). Internally it comprises crustal-scale half graben that are 6–15 km wide and tilt towards the E (Bell et al., 2014; Dreyer et al., 2005; Duffy, Bell, et al., 2015; Whipp et al., 2014) (Figure 3b). With the exception of a secondary NW-SE-striking fault population (Whipp et al., 2014), normal faulting within the Horda Platform largely pre- or post-dates the Late Jurassic (Dreyer et al., 2005; Holgate et al., 2013; Patruno et al., 2015; Whipp et al., 2014). The Måløy Slope is located N of the Horda Platform, is bound by the Øygarden Fault Complex to the E and shows a westward down-stepping of compartmentalized N-S striking half graben into the deep Sogn Graben (Jackson et al., 2008; Reeve et al., 2015).

4.2 | Lomre and Uer terraces

The Lomre and Uer terraces are down-thrown structures relative to the Horda Platform (Figure 3b). To the SE, the Lomre Terrace is bound by the Troll and Lomre South Fault (Figure 3b/c, TF, LSF). Further NE, the Lomre Terrace is bound by the Kinna Fault (KF) and a zone of closely spaced faults, which link the Kinna Fault with the Troll Fault. This fault transfer zone is characterized by narrow fault blocks (1–2 km wide) with NW- and SE tilt (Figure 3d). The Kinna Fault separates the eastward tilted Ryggsteinen Ridge (Figure 3c), a major intrabasinal horst, from the Lomre Terrace to the W and Uer Terrace to the E. The Uer Terrace is a comparably simple, 20-km-wide eastward tilted fault block, bound on its south-western side by the Vette Fault (Figure 3b).

The northern margin of the Lomre Terrace is the hanging wall of the Kinna Fault, and the western margin the faulted Flatfisk Slope that leads westward into the deep rift-axis of the North Viking Graben. The Sogn Graben is located to the N of the Lomre Terrace and separated from the North Viking Graben by the Marflo Spur (Figure 3) (Fossen et al., 2010).

5 | SEISMIC STRATIGRAPHIC FRAMEWORK

The seismic stratigraphic framework is based on six regional seismic horizons, tied to chronostratigraphic information from 40 wells (Figure 3). The mapped horizons divide the Late Jurassic interval into five stratigraphic units (Figure 2, SU1-5) with detailed age constraint provided by seismic well ties, allowing correlation with the J-sequences scheme of Partington et al. (1993). No direct well control was available for the Late Jurassic in the south-eastern Uer Terrace and the Flatfisk Slope. The eastern part of the study area, in particular the Måløy Slope, parts of the Uer Terrace, and the Ryggsteinen Ridge are heavily eroded and only remnants of the Late Jurassic stratigraphy are preserved, making seismic mapping of horizons difficult.

Horizon 1 forms the base of the Late Jurassic syn-rift interval and is picked on a major flooding event at the contact between Brent Group and the overlying Heather Formation. Horizon 1 varies significantly in phase and amplitude. It is most commonly a strong trough reflection, generated by moderate impedance Heather Formation mudstone against very low impedance coal seams within the deltaic Etive and Ness Formations, or low impedance transgressive sandstone of the Tarbert Formation (Table 1). Horizon 2 forms the top of Seismic Unit 1 and is mapped on a basin-wide maximum flooding surface (mfs) of late Callovian age (mfs J46, Partington et al., 1993), which also dates Seismic Unit 1 to mostly Callovian age.

The top of Seismic Unit 2 is defined by Horizon 3 and mostly mapped on a trough reflection marking the top of relatively thick intra-Heather Formation sandstones (Table 1). However, variations in phase do occur with sandstones showing peak, as well as trough reflectors at their top. Wells consistently date this horizon to the late mid Oxfordian (mfs J54, Partington et al., 1993), thus dating Seismic Unit 2 to early–mid Oxfordian (Figure 2).

Horizon 4 forms the boundary between Seismic Units 3 and 4 and is dominantly mapped on a strong to moderate peak reflection caused by mud-rich strata overlying relatively thin gravity flow deposits (Table 1). However, phase can vary for

TABLE 1 Details of mapped seismic horizons

Seismic horizon	Dominant polarity	Approximate age	Comments
6. Top Draupne Fm./BCU	Trough	Late Tithonian	Strong regional reflector caused by sharp downward decrease from carbonaceous Lower Cretaceous into low-impedance mudstone of Draupne Formation
5. Base Draupne Fm.	Peak	Late Kimmeridgian – Early Tithonian	Regional reflector from low-impedance Draupne Formation mudstone to underlying moderate-impedance Heather Formation mudstone
4. Intra-Heather Fm./Base Canyons	Peak	Late Oxfordian – Early Kimmeridgian	Local strong amplitude, mostly peak, due to impedance contrast of intra-Heather sandstone against Heather Fm. mudstone
3. Intra-Heather Fm.	Trough	Middle Oxfordian	Dominantly trough response from thick low-impedance intra-Heather Fm. sandstone against overlying moderate to high impedance Heather Fm. mudstone
2. Intra-Heather Fm.	Peak	Late Callovian	Regional trough caused by upward increase of impedance caused by Callovian maximum flooding event
1. Top BRENT Gr.	Trough	Bajocian – Early Callovian	Frequent-phase variation but usually strong trough caused by very low-impedance coal of Ness Formation, regionally approximates base syn-rift

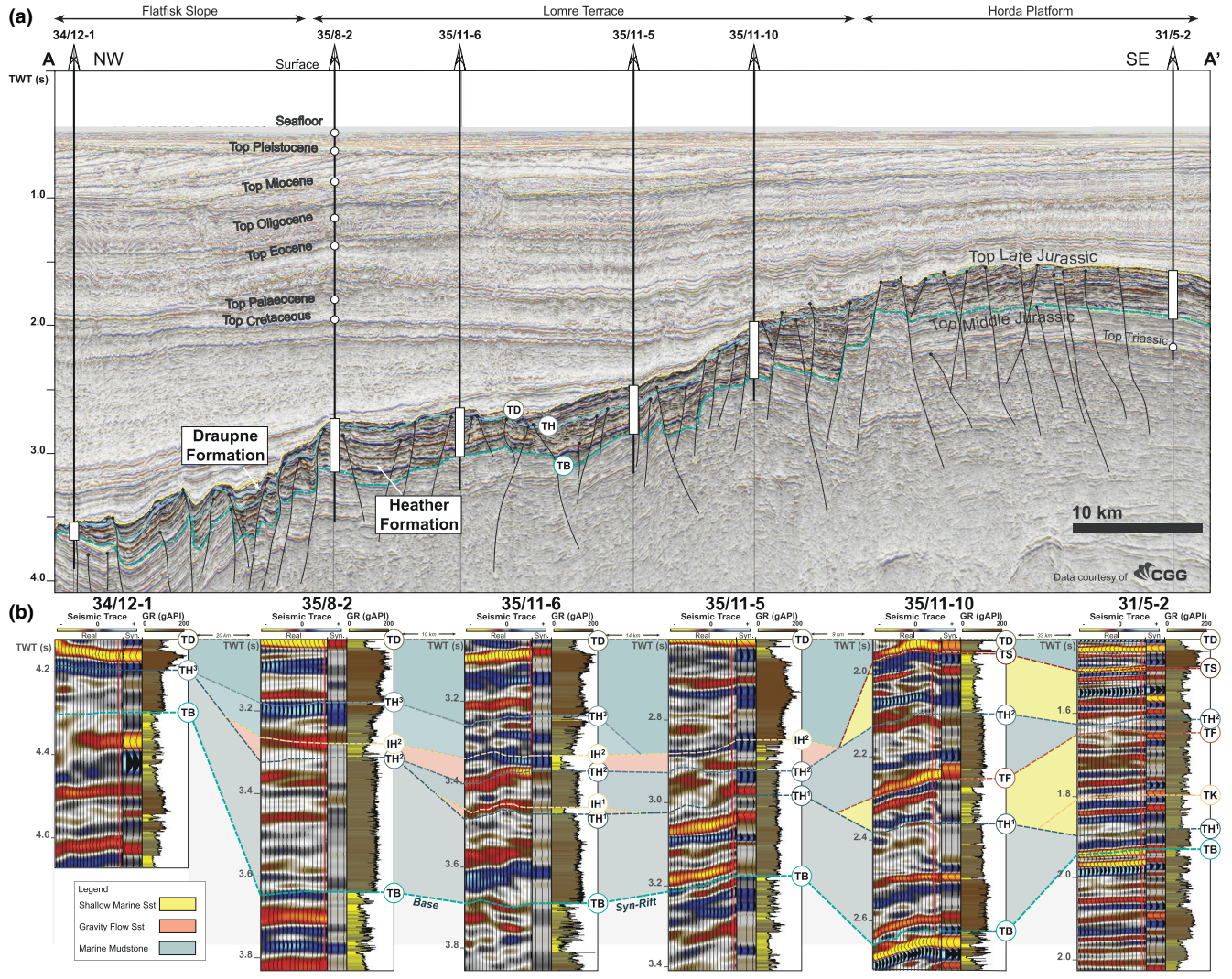

FIGURE 5 Well correlation panel through the study area (location in Figure 3). (a) Seismic line through well locations on Horda Platform in SE (right-hand side), Lomre Terrace (centre), and Flatfisk Slope in NW (left-hand side). (b) Wells from (a) with real seismic trace around the well, synthetic seismogram for seismic well tie, and gamma ray log of Late Jurassic stratigraphy. Lithostratigraphic Tops: TB = Top BRENT, TH^1 = Top Heather Fm. I, IH^1 = Intra-Heather Fm. Sst., TK = Top Krossfjord Fm., TF = Top Fensfjord Fm., TH^2 = Top Heather Fm. II, IH^2 = Intra Heather Fm. Sst., TS = Top Sognefjord Fm., TH^3 = Top Heather Fm. III, TD = Top Draupne Fm

this horizon, which is in some areas represented by a trough reflection. Age data from wells define the surface as latest Oxfordian and early Kimmeridgian age (mfs J62, Partington et al., 1993).

Horizon 5 marks the top of Seismic Unit 4 and was mapped on a very strong regional peak reflection at the base of Draupne Formation mudstone. This contact is conformable in most parts of the Lomre Terrace and hangingwall of the Kinna Fault, but local truncation occurs on structural highs, especially the Uer Terrace and Ryggsteinen Ridge, where Seismic Unit 4 is almost completely absent. Well ties suggest that mudstone overlying Horizon 5 give an earliest Tithonian age and that Horizon 5 equates to the J64 mfs (Partington et al., 1993). Hence, Seismic Unit 4 is of early-to-late Kimmeridgian age.

A very strong regional trough reflection caused by calcareous Lower Cretaceous strata on top the Draupne Formation mudstone marks Horizon 6, which defines the top of Seismic Unit 5 (Table 1). Horizon 6 was mapped on this basin-wide seismic event, which is referred to as Base Cretaceous Unconformity (BCU), and approximates the J74 mfs (Partington et al., 1993) in areas of correlative conformity.

6 | LITHOSTRATIGRAPHIC FRAMEWORK

Figure 5 is a well section from the Horda Platform across the Lomre Terrace and onto the Flatfisk Slope and is used to provide the Late Jurassic depositional environment framework of the study area. Well 31/5-2, located on the Horda Platform, contains all three Late Jurassic deltaic formations (the Krossfjord, Fensfjord, Sognfjord formations; Patruno

et al., 2015; Stewart et al., 1995), separated by transgressive intervals characterized by high-gamma ray Heather Formation mudstone.

The most proximal well on the Lomre Terrace 35/11-10 (Figure 5) also contains more than two hundred meters of the deltaic Fensfjord and Sognefjord Formation, but also much thicker Heather Formation mudstone. Mudstone dominated, high-gamma ray strata in 35/11-5 indicates the transition from overall shallow marine to slope environments in the proximal to central Lomre Terrace W of 35/11-10 and 35/11-4 (Ravnås et al., 2000). 35/11-5, together with other north-westerly wells (35/11-6, 35/8-2, 34/2-1; Figure 5), is dominated not only by high-gamma ray mudstone, but also shows that low-gamma ray deposits occur in the central Lomre Terrace and the hanging wall of Kinna Fault (e.g. 35/8-2, 35/11-6, 35/11-5). These deposits have informally been referred to as intra-Heather Formation sandstones (Koch et al., 2017; Zhong et al., 2020). They are cored in several wells on the Lomre Terrace (Figure 4), and interpreted as gravity flow deposits and hyperpycnites (Ravnås et al., 2000; Zhong et al., 2020). Wells from the Ryggsteinen Ridge (35/9-8, 35/9-7, 35/9-10A; Figure 4) contain several intervals of Late Jurassic intra-Heather sandstones, which have been interpreted as stacked low-density to high-density gravity flow deposits with occasional argillaceous, mud clast-bearing linked debrites (Koch et al., 2017). In contrast, strata on the long-lived Late Jurassic intra-basin high on the Flatfisk Slope are condensed and dominated by high-gamma ray mudstone (well 34/12-1).

7 | WELL-CALIBRATED SEISMIC FACIES

We identify six seismic facies (Table 2), calibrated by well-based sedimentological data (Figures 6–11), that characterize the Late Jurassic of the Lomre and Uer Terraces: (1) channelized lobes, (2) fault-confined lobes, (3) submarine channel belts, (4) proximal submarine canyons, (5) distal submarine canyons and (6) background deposition. Seismic Facies 1 and 2 occur contemporaneously and are overlain by the younger Seismic Facies 3. They are part of a prograding slope that developed on the fault terraces basinward of the Sognefjord delta. Seismic Facies 4 and 5 are younger features and occur stratigraphically above Seismic Facies 1–3.

7.1 | Seismic Facies 1. Channelized lobes

7.1.1 | Seismic expression

Seismic Facies 1 (SF1) is part of the first, and volumetrically most important gravity flow interval in the study area with overall sandstone thicknesses above 100 m. Seismic Facies 1 dominantly occurs in the hanging wall of the Kinna Fault and extends towards the W and NW onto the Marflo Spur and Flatfisk Slope (Figure 3b). In cross section, SF1 does not show significant seismic-scale basal truncation and the top usually corresponds to a semi-continuous trough reflection, but can also sit within a prominent peak reflector, as in 35/11-6 (Figure 6a; Table 2). Internal reflectors are of very low frequency with massive, internally chaotic bedding. Plan-view attribute patterns consist of numerous patchy amplitudes that appear as amalgamated lobate shapes and reoccurring, ca. 0.5-km-wide ribbon-shaped dimming that suggest channelized pathways (Figure 6c). Neither lobes nor ribbons seem to clearly converge into a common up-dip feeder point.

7.1.2 | Core-log calibration

Seismic Facies 1 is penetrated by well 35/11-6 (Figure 6). The well contains ca. 40-m-thick sandstone stratigraphy, characterized by a box-shaped low-gamma ray interval, generally high resistivity and density-neutron log crossover between 3,157 and 3,196 m MD (Figure 6a). This interval is stratigraphically located within SF1, with its top surface about 10 m above the presumed shale-sand interface. About 30 m of core calibrate the low-gamma ray interval as mostly massive fine- to medium-grained sandstones, separated by thin interbeds of dark grey claystone and siltstone (Figure 6b/c). Sandstones are generally massive, have erosive bases with rip-up clasts and occasionally exhibit fining upwards trends. A sharp-based breccia with irregular mudclasts (3172–3174 m MD) was interpreted as linked debrite, as described in e.g. Haughton et al. (2003), indicating a relatively central position within the overall gravity-flow complex. Slightly more proximal wells 35/11-13 and -14S (Figure 6d/Figure 12a) contain over one hundred meters of time-equivalent sandstones (Table 2, SF1 cross-section). Well 35/11-15S, located in the immediate hanging wall of the Kinna Fault (Figure 6d/Figure 12a) contains 195 m of sandstone strata.

7.1.3 | Interpretation

The massive sandstones are interpreted as amalgamated high-density fractions of erosive gravity flows, whereas the fining-upward intervals suggest more gradual decrease in flow energy and subsequent preservation. These cored deposits are likely deposited from submarine channels in a bigger, very sand-rich submarine lobe complex that extends much further towards the W and NW (e.g. well 35/8-2, Figure 7a). Strata in well 35/11-15S and 35/11-13 have generally been interpreted, based on core sedimentology, as amalgamated high-density gravity flows deposited in a structurally confined channelized lobe system with associated channel margin and overbank deposits, which partly

TABLE 2 Details of the six seismic facies observed in the Late Jurassic, based on reflector character, depositional geometry, well-log characters and plan-view seismic geomorphology

Seismic facies *(dominant age)*	Reflector character	Depositional geometry	Seismic section with gamma ray & acoustic impedance log (scale bar = 100 ms) GR (gAPI) AI (kPa*s/m)	Plan-view attribute character (scale bar = 5 km) & location of seismic section
1. Channelized lobes *(J52–J54)*	Semi-continuous to chaotic high amplitude trough at top, very low frequency internal reflections, frequent low amplitude to transparent internal reflections	Thick sand-rich gravity flow deposits with generally low impedance, massive internally chaotic bedding, plan-view character shows unconfined patchy amplitudes with occasional internal channelization	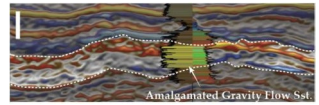	
2. Fault confined lobes *(J52–J54)*	Continuous trough at top, brightening along dip slope, internal phase variations on semi- to discontinuous reflectors, bright lenses proximal to fault plane	Wedging geometry into hanging walls of antithetic faults, onlap on dip slopes and fault monocline, plan-view shows subtle fault-axial patterns, common sharp amplitude termination against fault planes	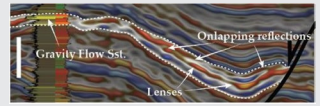	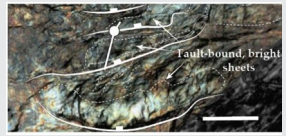
3. Submarine channel belt *(J54–J62)*	Semi-continuous, low- to high-amplitude reflectors of higher frequency, dominantly draped by low frequency, high amplitude peak, occasional phase change with thinning	Base partly truncating, partly conformable, internal stacked reflectors and lenses, low gamma ray gravity flow deposits of varying impedance, plan-view shows transverse ribbon shaped patterns and surrounding high amplitude sheets	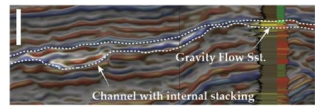	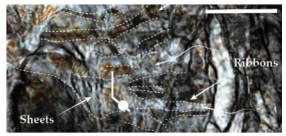
4. Proximal submarine canyon *(J62–J64)*	Basal continuous, low-frequency, high-amplitude peak reflector, overlain by discontinuous, low-amplitude reflections	Base surface truncates underlying strata, lower fill onlaps onto truncation, upper transparent strata dominantly draping character, plan-view shows dendritic drainage pattern	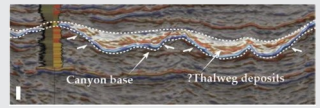	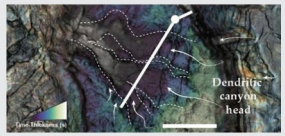
5. Distal submarine canyon *(J62–J64)*	Basal continuous, low-frequency, very high-amplitude peak reflector, overlain by high-amplitude trough reflections	Base surface truncates underlying strata, fill dominantly draped high gamma ray shale, basal low gamma ray/high impedance gravity flow deposits in thalweg, plan-view confined sinuous pattern	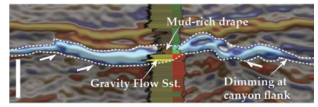	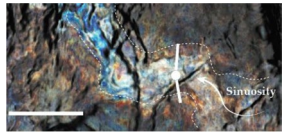
6. Background deposits *(J36–J76)*	Continuous low- to high-amplitude reflectors, low to high frequency	Parallel stack, partly very high-gamma ray shale with very low impedance, generally draping geometry, plan-view shows smooth pattern	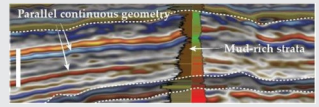	

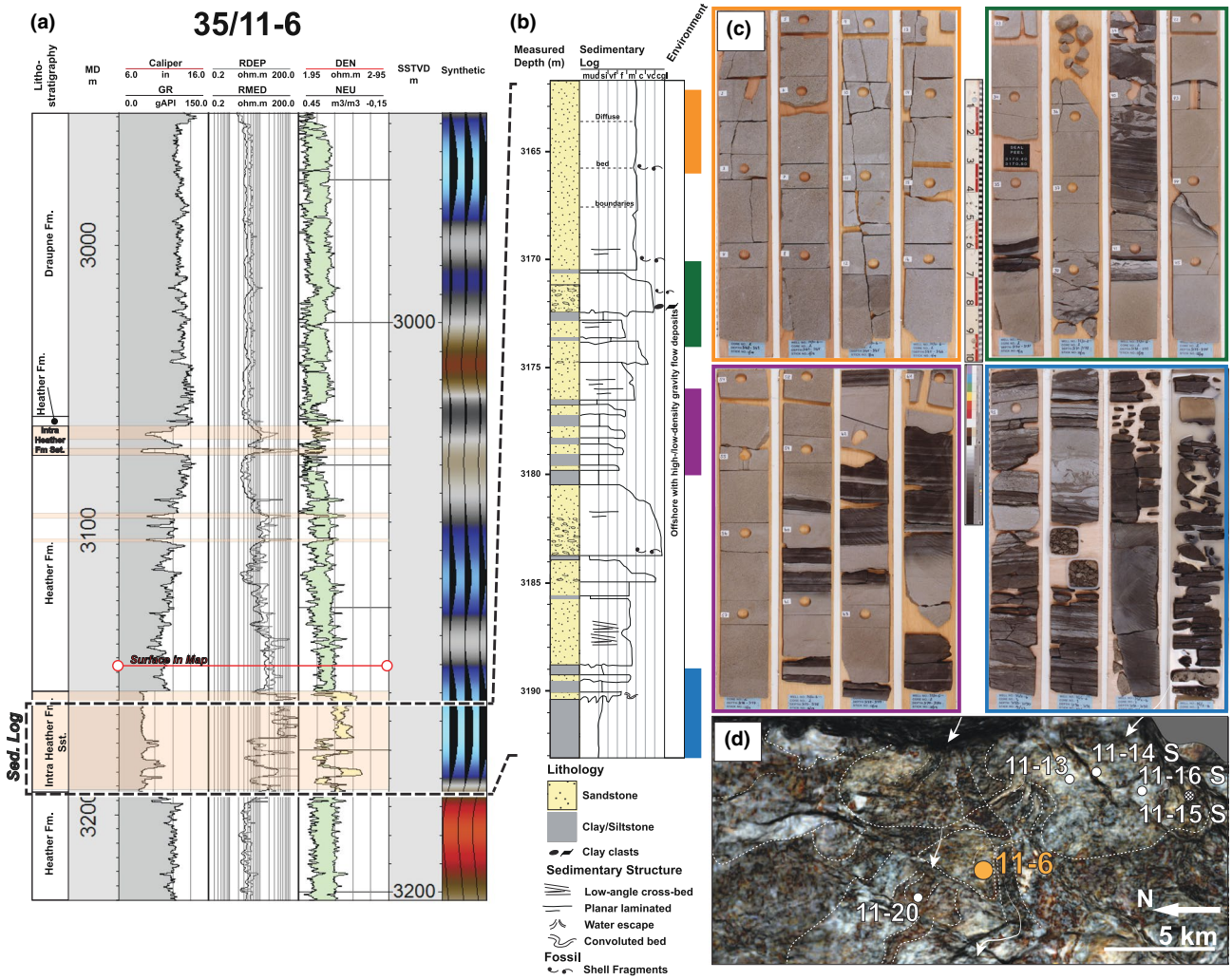

FIGURE 6 Well 35/11-6. (a) Well-log data for the Viking Group comprising gamma ray, resistivity, neutron and density logs. Interpreted gravity flow deposits marked by transparent orange overlay. Location of cored and logged interval marked by dashed line. (b) Core description re-drawn from McAndrew (2010) with (c) selected examples of core photos (position colour coded next to sedimentary log). (d) Amplitude map of Seismic Facies 1 showing the location of 35/11-6 (orange)

cannibalize precursor deposits (Bakke et al., 2013; Zhong et al., 2020).

We suggest that the patchy depositional architectures are caused by overlapping, clustered compensational lobes (Stow & Mayall, 2000) and that the internal ribbon shapes are caused by intralobe distributary channels and incision of larger feeder channels (Prélat et al., 2009; Saller et al., 2008). The overall chaotic appearance of SF1 indicates a sedimentary fairway with a significant component of amalgamation and cannibalization, where younger feeder channels incise into older lobes (Saller et al., 2008).

7.2 | Seismic Facies 2. Fault-confined sheets

7.2.1 | Seismic expression

Seismic Facies 2 (SF2) is also part of the first, and volumetrically most important gravity flow interval in the study area (Table 2). Seismic Facies 2 dominantly occurs in narrow, fault-bound depocenters in the northern Lomre Terrace, S of the hanging wall depocenter of the Kinna Fault (Figure 3b/Figure 8d). In cross-section, SF2 usually displays a distinct wedge-shaped geometry that thickens into the immediate hanging wall of SE-/NW dipping normal faults and shows internal onlap onto the hanging wall dipslope. The top of SF2 is typically characterized by a strong continuous trough, whereas internal reflections can vary in phase and frequency but are overall continuous. Some reflections show bright lenses, at the limit of seismic resolution, ca. 15 ms (TWT) (ca. 25 m) thick, which are most prominent in close proximity to the normal fault. In cross-section, as well as in plan-view, SF2 is generally characterized by distinct brightening down the dipslope of the 2–6 km wide fault blocks and highest amplitudes in the immediate hanging wall. The amplitudes are sheet-like in plan-view with little internal morphology, although subtle fault-parallel lineation can sometimes be observed.

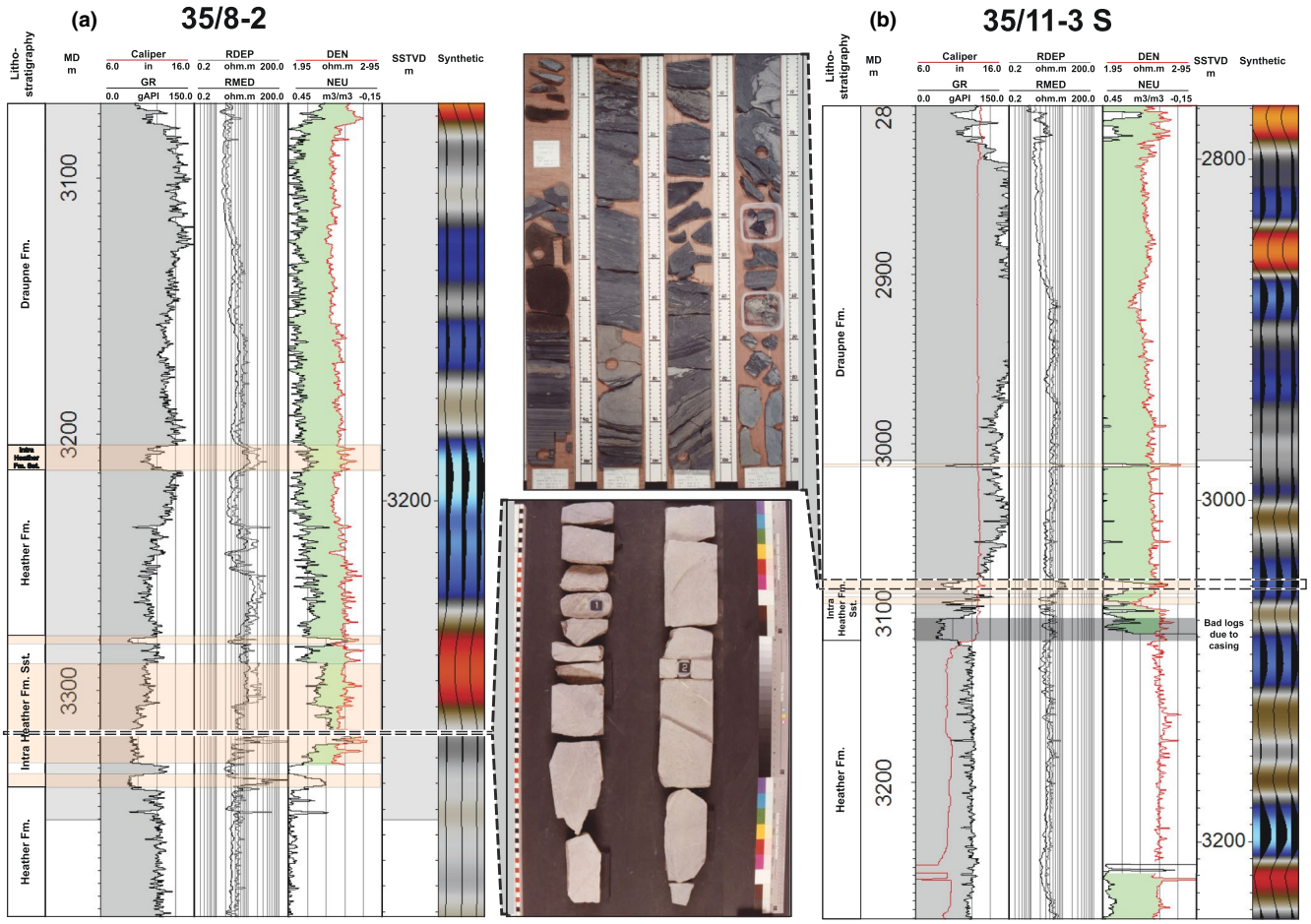

FIGURE 7 Wells with cored Late Jurassic gravity flow strata. (a) Well-log data from 35/8-2 for the Viking Group comprising gamma ray, resistivity, neutron and density logs. Interpreted gravity flow deposits marked by transparent orange overlay. Location of cored interval marked by dashed line. (b) Well-log data from 35/11-3S for the Viking Group comprising gamma ray, resistivity, neutron and density logs. Location of cored interval marked by dashed line

7.2.2 | Core-log calibration

A core from 35/11-9 penetrates a particularly reflective part of SF2 on the northern Lomre Terrace (Figure 8a–c). The box-shaped well-log character and core indicate two major sandstone intervals between 2,650 and 2,740 m. Both sandstones are mostly structureless and unbioturbated. Internally, the lowermost sandstone is characterized by several coarsening- to fining-upward packages (2,732–2,703 m MD; Figure 8b), whereas the uppermost interval consists of several sharp-based, fining upward packages (2,692–2,653 m MD; Figure 8b). The mudstone occurring below and between the sandstone intervals are ca. 4–8 m thick and bioturbated to a varying degree. Some crestal wells (e.g. 35/11-3S; Figure 7b) contain several thin (ca. 5 m), low-gamma ray intervals of high and low impedance, comparable to cored gravity-flow deposits observed in adjacent wells.

7.2.3 | Interpretation

The lowermost sandstone packages sharply overlies strongly bioturbated, dark-grey siltstones, which we infer were deposited in well-oxygenated, open marine conditions (see Holgate et al., 2013, 2015). In contrast, overlying mudstones are only weakly bioturbated, suggesting they were either deposited in; (i) a relatively proximal position, in which turbulent, sediment-rich, brackish-water conditions occurred due to the frequent input from basin-margin deltas (Ekdale et al., 2012); or (ii) a relatively distal, deeper-water, poorly oxygenated setting (Ekdale et al., 2012). Due to the mostly massive and structureless bedding, we infer both sandstones were deposited by high-density turbidity currents (e.g. Haughton et al., 2009).

The disparity in terms of seismic reflector character between elevated footwalls and down-thrown hanging walls suggests an influence of fault-controlled topography on deposition of SF2. Wells such as 35/11-9 calibrate that these fault-confined, high-amplitude sheets as areas containing coarse-grained sandstone strata. We suggest that the ponded depocenters on the rifted slope have likely captured coarse-grained gravity flow deposits of SF2 in asymmetric, fault-controlled depressions (Anderson et al., 2000; Kane et al., 2010). Draping, continuous, high-amplitude, low-frequency reflections are, however, a prominent feature of SF2, suggesting hemipelagic deposits as a major component of this seismic facies.

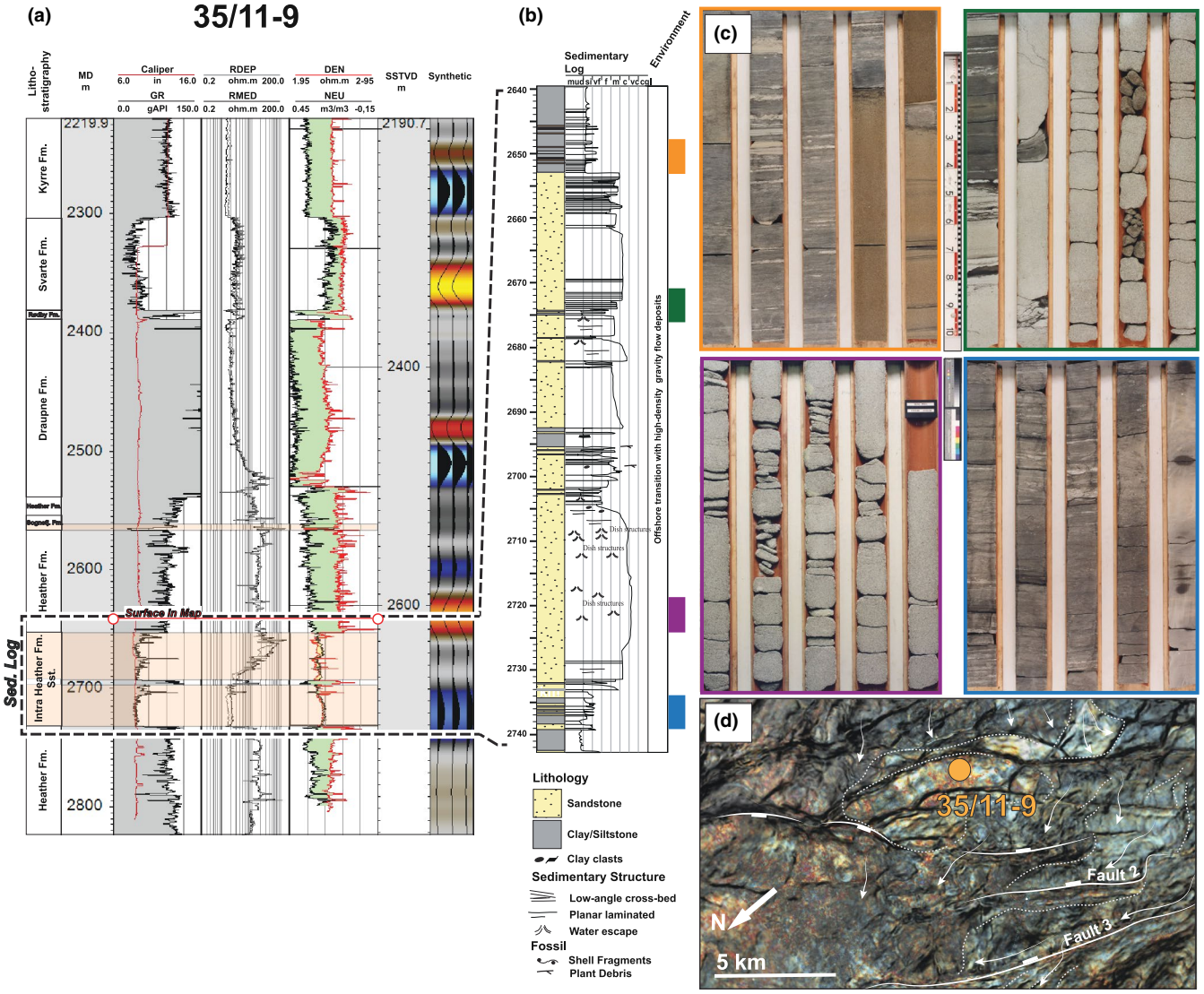

FIGURE 8 Well 35/11-9. (a) Well-log data for the Viking Group comprising gamma ray, resistivity, neutron and density logs. Interpreted gravity flow deposits marked by transparent orange overlay. Location of cored and logged interval marked by dashed line. (b) Core description re-drawn from McAndrew (2010) with (c) selected examples of core photos (position colour coded next to sedimentary log). (d) Amplitude map of Seismic Facies 2 showing the location of 35/11-9

7.3 | Seismic Facies 3. Submarine channel belt

7.3.1 | Seismic expression

Seismic Facies 3 (SF3) is part of the second significant gravity flow interval in the study area, which contains thinner gravity flow strata than SF1 and SF2 with sandstone thickness generally <40 m. Seismic Facies 3 stratigraphically overlies SF1 and SF2. It dominantly occurs in the southern part of the hanging wall of the Kinna Fault, in the northern Lomre Terrace and extends onto the southern edge of the Marflo Spur and Flatfisk slope (Figure 3b). In cross section, SF3 is characterized by local strong peak responses at its top and internal heterogeneous stacking of strata is suggested by prominent phase/amplitude variation of internal reflections (Table 2). In plan-view, SF3 is defined by relatively narrow, 0.8–1.6 km wide, ribbon-shaped amplitude anomalies that are sub-parallel in proximal locations and converge down-dip into sheet-like high-amplitude areas (Figure 9d). These amplitudes, however, often contain dimmed ribbon-shaped geometries (SF3 plan-view, Table 2). Overall, SF3 is spatially more confined than SF1 and SF2.

7.3.2 | Core-log calibration

Well 35/11-5 penetrates SF3, showing it corresponds to a ca. 44-m-thick interval containing several 0.5- to 2-m-thick

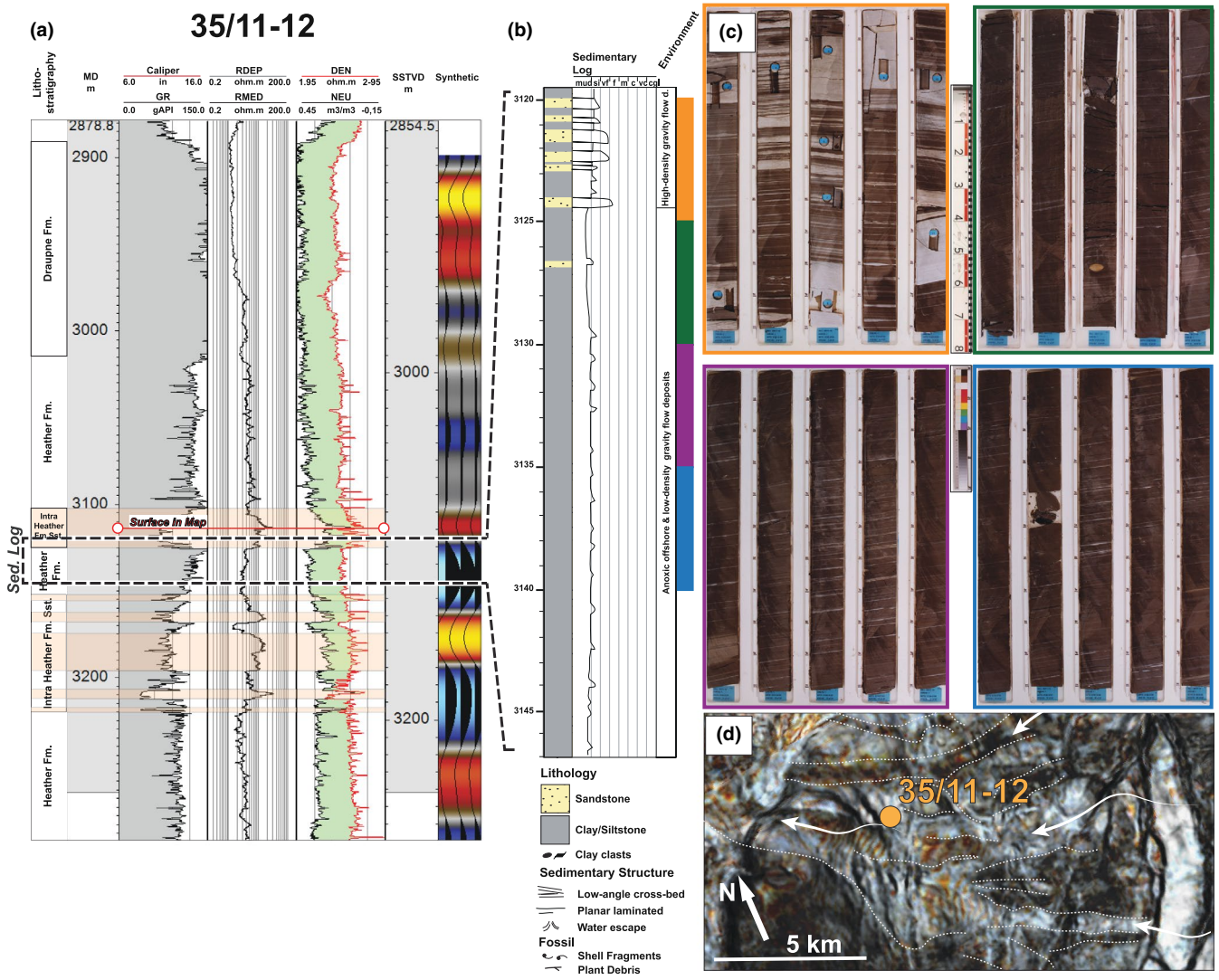

FIGURE 9 Well 35/11-12. (a) Well-log data for the Viking Group comprising gamma ray, resistivity, neutron and density logs. Interpreted gravity flow deposits marked by transparent orange overlay. Location of cored and logged interval marked by dashed line. (b) Core description re-drawn from McAndrew (2010) with (c) selected examples of core photos (position colour coded next to sedimentary log). (d) Amplitude map of Seismic Facies 3 showing the location of 35/11-12

beds, characterized by sharp-based, low-gamma ray and low acoustic impedance (Table 2). This log expression is similar to high-density gravity flow deposits cored in other wells on the Lomre Terrace. Well 35/11-12 is located in the axis of SF3 and stratigraphically located within a bow-shaped, low-gamma ray interval (Figure 9a). Core at the very base of this interval contains thin, massively graded sandstones (Figure 9b/c), which suggests that the 25-m-thick overlying interval contains significant sand-rich strata as well.

7.3.3 | Interpretation

The sandstone strata in well 35/11-12 was interpreted to derive from relatively high-density gravity flows due to the lack of grading within the sandstone beds. Well log character and mud logging descriptions indicate more sandstone strata above the cored interval, which suggests that the core captures the base of >25-m-thick gravity flow deposits. The underlying mudstone contains thin siltstone beds, which we interpret as hemipelagic-dominated slope deposits with slightly coarser-grained layers. Together with the ribbon-dominated plan-view geomorphology of SF3 we interpret that these deposits represent a submarine channel belt. Areas of SF3 that show few ribbon geometries, but dominant sheet-like amplitudes, may show overbank deposits and transient lobes on the terraced slope (Stow & Mayall, 2000). The general low sinuosity of SF3 together with a lack of levee build-up might suggest a relatively sand-rich systems (Galloway, 1998; McHargue et al., 2011). Sand-rich gravity flow system commonly preserve low rates of overbank aggradation and thin channel elements that overfill and splay out rapidly (McHargue et al., 2011; Posamentier & Kolla, 2003).

7.4 | Seismic Facies 4. Proximal submarine canyons

7.4.1 | Seismic expression

Seismic Facies 4 (SF4) is located on the northernmost Lomre Terrace and the western Uer Terrace (Figure 3b) and is stratigraphically younger than SF1, SF2 and SF3. In cross section, SF4 shows U-shaped, canyon-like incision into underlying stratigraphy with flanks dipping between 10° and 20°. The maximum depth of incision occasionally exceeds 200 ms (TWT) (ca. 336 m; Figure 10a). The canyon internal strata are characterized by generally parallel, low-amplitude reflections with onlap onto the basal truncation surface (Figure 10). No slumped geometries above seismic resolution were observed. The upper part of the infill has a generally low amplitude with a draping geometry and shows subtle parallel internal character. In plan-view, SF4 is characterized by valleys that are 2.5–3-5 km wide and 10–25 km long. Up-dip the canyons have a dendritic plan-view geometry (Figure 10b).

7.4.2 | Well calibration

No well directly penetrates the proximal canyons. The strong reflection at the base of the canyon can, however, be traced up-flank to a well position and ties it to a downward impedance increase from high-gamma ray mudstone to underlying strata.

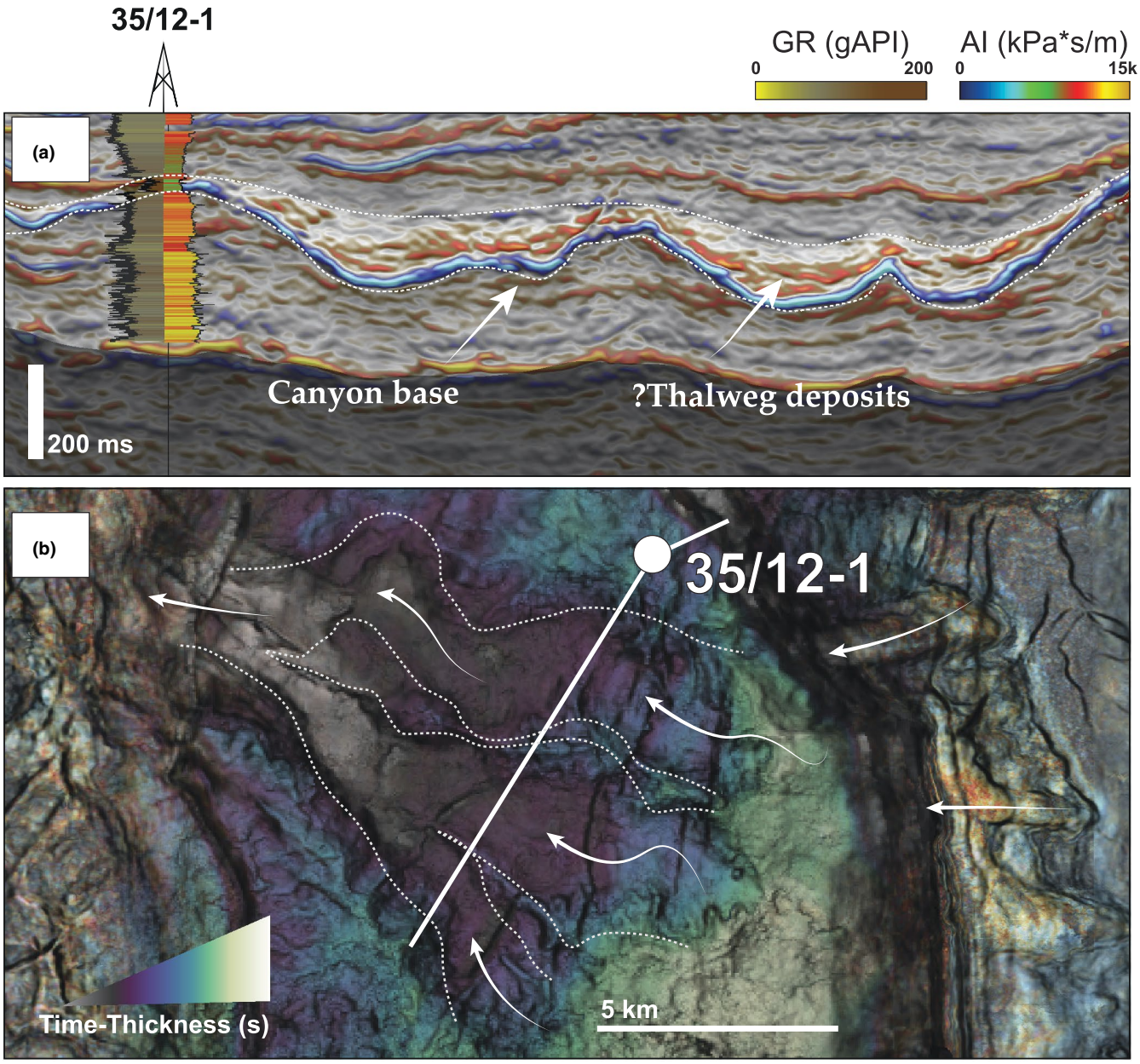

FIGURE 10 Seismic expression of Seismic Facies 4 in cross section and map-view

Since the canyon fill is not calibrated by well data, no confident prediction of the lithology can be made. The reflection variation in phase and amplitude of the lower canyon fill suggests stacking of heterogeneous layers (Figure 10). Their cross-section form shows broad, shallow, channel-like geometry. However, these patterns are not persistent along the canyon axis to the NW. The proximal canyons pass downdip into Seismic Facies 5.

7.4.3 | Interpretation

We have interpreted these valley-like erosion features as submarine canyons based on the geomorphology, their relationship to other seismic facies and the regional context. The seismic expression of SF4 correlates well with submarine canyon described on the Måløy Slope, northward of the Lomre and Uer Terraces (Jackson et al., 2008, 2019; Sømme et al., 2013). The dendritic plan-view expression to the E is interpreted as relating to the canyon heads in SF4, hence the terminology of *'proximal'* submarine canyon. The amplitude variation and canyon fill geometries, albeit being very discontinuous, imply sedimentary processes other than just hemipelagic sedimentation. The lower canyon fill could have derived from aggradational, low-density gravity flows or slumped canyon flanks, as suggested by other seismic studies of submarine canyons (e.g. Deptuck et al., 2007; Mayall et al., 2006). In contrast, the upper transparent canyon fill is interpreted as dominated by hemipelagic and dilute gravity flow deposits during the gradual abandonment of canyons as active sedimentary pathways.

7.5 | Seismic Facies 5. Distal submarine canyons

7.5.1 | Seismic expression

Seismic Facies 5 (SF5) occurs downdip and in continuation of the proximal submarine canyon (SF4) on the deep-water fault terraces. However, depth of incision, reflection character and plan-view geometry show significant differences allowing discrimination from their up-dip counterparts. Seismic Facies 4 is defined in cross-section as high-amplitude peak reflection. The depth of truncation is less pronounced than SF4 and often below vertical seismic resolution, especially in distal parts of the fairway. On the Lomre Terrace, channel-like cross-section geometry of SF5 is less than 50 ms (TWT) (ca. 80 m) deep and flanks slope at a lower angle (<5°) than SF4 (Table 2). In plan-view SF5 has a sinuous pattern with an approximate wavelength of 7–10 km and a sinuosity of typically 1.2–1.3. The sinuous amplitudes of SF5 are 5–7 km wide and could extend more than 40 km down-dip into the North Viking and Sogn Graben.

7.5.2 | Core-log calibration

Well 35/11-2 intersects SF5 ca. 10 km downstream of its transition from SF4, which occurs across the Kinna Fault (Figure 11b/c). Cores through SF5 strata have low-gamma ray values, which suggests the presence of about 30 m of gravity flow sandstones (Figure 11a). The gamma ray log character is bell shaped, suggesting a gradual fining upward trend for the canyon fill at the well position. The core of 35/11-2 is only about 3 m long but captures a coarse- to very coarse-grained 0.5-m-thick, massive sandstone with erosive base as likely basal stratigraphy of the canyon fill. The massive sandstone is overlain by three, 0.3-m-thick, erosive-based fining-upward sandstone beds. These beds have coarse- to medium-grained sandstones at the base with planar laminated silt to dark grey mudstone strata at the top.

7.5.3 | Interpretation

We interpret the deposits cored by 35/11-2 as stacked gravity-flow deposits, which are interbedded with offshore mudstones. The erosive base and massive bedding of the lowermost sandstone indicates a high-energy flow. The persistent fining upwards trends of upper sandstones indicate low-density gravity flow deposits (Haughton et al., 2009). The low-gamma ray strata above the core are likely sandstones with an overall fining upwards trend, as suggested by gradual increase of the gamma ray values towards the top of SF5 (Figure 11a).

The regional seismic surface displayed in the amplitude map (Figure 11d) intersects 35/11-2 strata on top of the overall fining-upward sequence and likely images the high-amplitude reflection caused by the impedance contrast between the mud-dominated upper canyon fill against the gravity-flow sandstone strata of the lower canyon fill. Based on the interpretation of the cored sediment and seismic geomorphology, we interpret this seismic facies as distal submarine canyon (cf. Deptuck et al., 2007). The increased sinuosity and decreased truncation depth, compared to SF4, may reflect gentler slope gradients on the terraced slope or decreased flow energy for SF5. We interpret the lack of seismically resolvable aggradational architectures within SF5, such as inner levees or channel forms, as an indication for a bypass dominated canyon. However, relatively thin coarse-grained, aggradational gravity flow deposits (ca. 20 m) are possible, as proven by well 35/11-2 (SF5 cross section, Table 2).

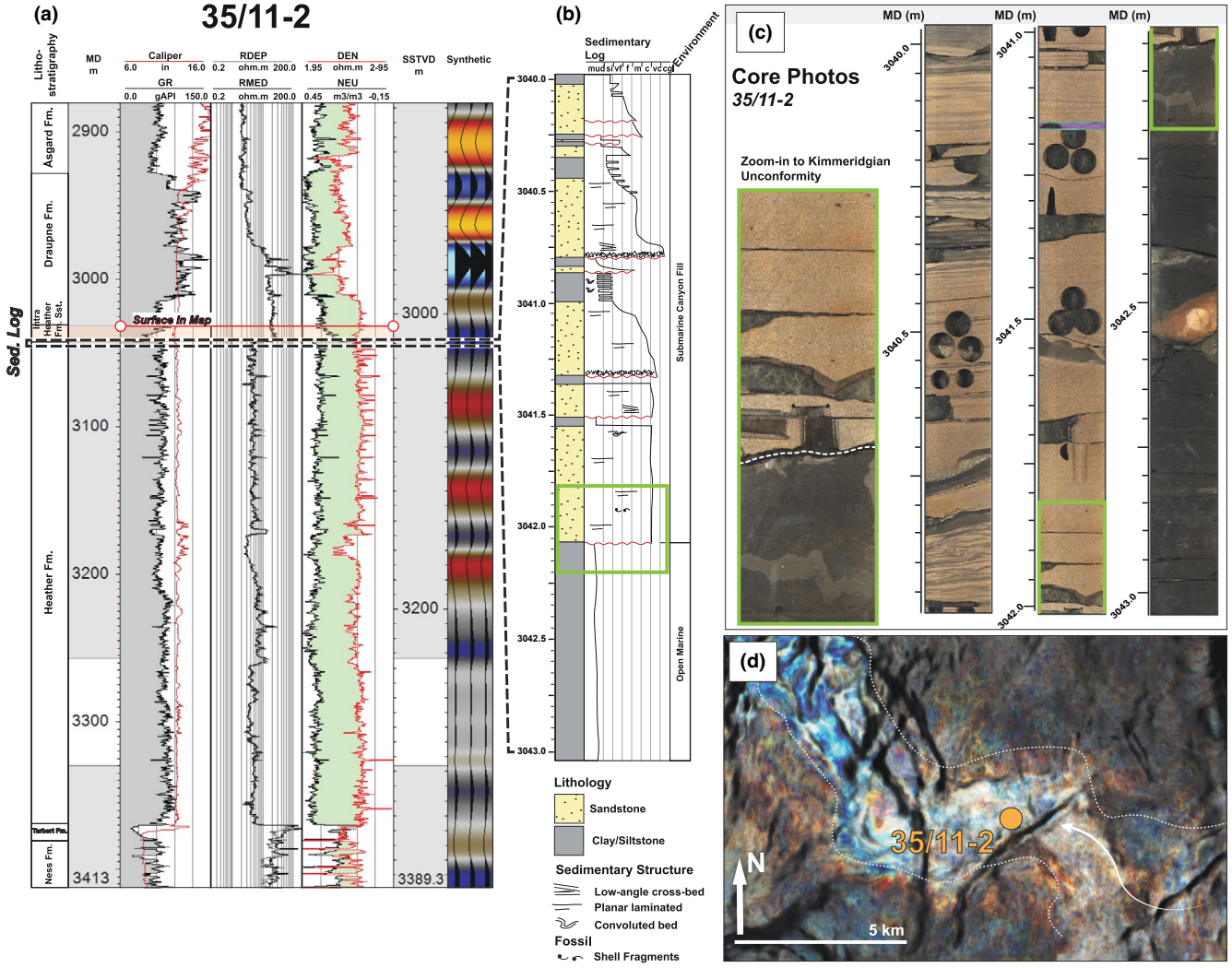

FIGURE 11 Well 35/11-12. (a) Well-log data for the Viking Group comprising gamma ray, resistivity, neutron and density logs. Interpreted gravity flow deposits marked by transparent orange overlay. Location of cored and logged interval marked by dashed line. (b) Core description re-drawn from McAndrew (2010) with (c) selected examples of core photos (position colour coded next on sedimentary log). (d) Amplitude map of Seismic Facies 5 showing the location of 35/11-2

7.6 | Seismic Facies 6. Background deposits

7.6.1 | Seismic expression

Seismic Facies 6 (SF6) is volumetrically the most important seismic facies in the study area (Table 2). It is deposited across the entire study area, contemporaneous with all other seismic facies. In cross section, SF6 is characterized by mostly parallel to divergent continuous reflections of varying frequency and amplitude (Table 2).

7.6.2 | Core-log calibration

The impedance within SA6 is generally low to moderate and gamma ray readings moderate to very high. Cores from exploration wells are generally biased towards sandstone strata, which means that there are no dedicated cores for SF6. However, mudstone strata that is intercalated in, or bounding the base of sandstone strata in all of the previously mentioned cores (Figures 6–11), can be used as calibration for the mud-dominated lithology of SF6.

7.6.3 | Interpretation

SF6 correlates with the Draupne and Heather Formation mudstone, which are the background strata in which the gravity flow deposits of SF1-SF5 are embedded in. The parallel bedding and mud-dominated lithology suggests low-energy environments where mud particles can settle and fall out from the water column. The dominant depositional processes for SA6 are likely unconfined, very dilute gravity flows and suspension settling (e.g. Stow & Mayall, 2000).

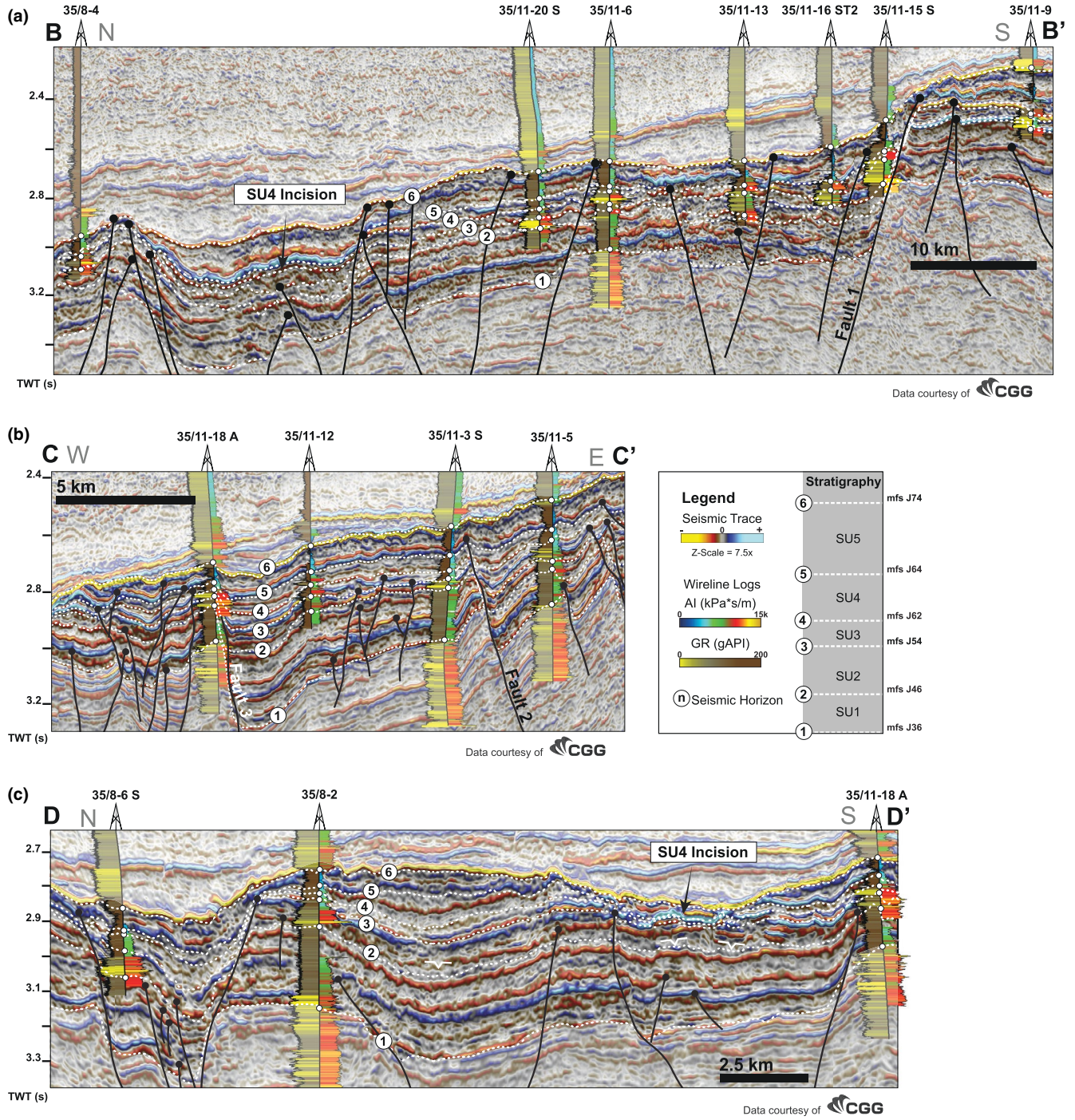

FIGURE 12 Seismic sections through key wells of the studies stratigraphy on the Lomre Terrace and hanging wall of the Kinna Fault (locations in Figures 13–17). The seismic data are displayed in SEG reverse polarity convention, whereby a downward increase in acoustic impedance results in a peak response (blue reflector), wireline logs are 1) gamma ray and 2) acoustic impedance

8 | SEISMIC SYN-RIFT UNITS

In this section we describe sediment thickness distribution (Figures 13a–17a) and attribute maps (Figures 13b–17b) of the five seismic units in order to analyse the Late Jurassic syn-rift deep-water sediment routing systems. Interpretations in eroded areas such as the Ryggsteinen Ridge have been 'interpolated' from surrounding stratigraphic remnants, where preserved. Simplified palaeogeographical reconstructions are summarized for each unit in Figure 18.

8.1 | Seismic Unit 1: (Bathonian–late Callovian; ?J32–J46)

Seismic Unit 1 (SU1) is bound by Horizons 1 and 2, is Bathonian–late Callovian in age and dominated by background slope deposits (SF6). It shows strong lateral variation in time thickness (Figure 13a). Overall, SU1 thickens towards the N/NW and generally ranges from 0.1 to 0.2 s (TWT), and locally up to 0.3 s (TWT) in some N- to NE-trending, fault-bounded hanging wall depocenters on the northern

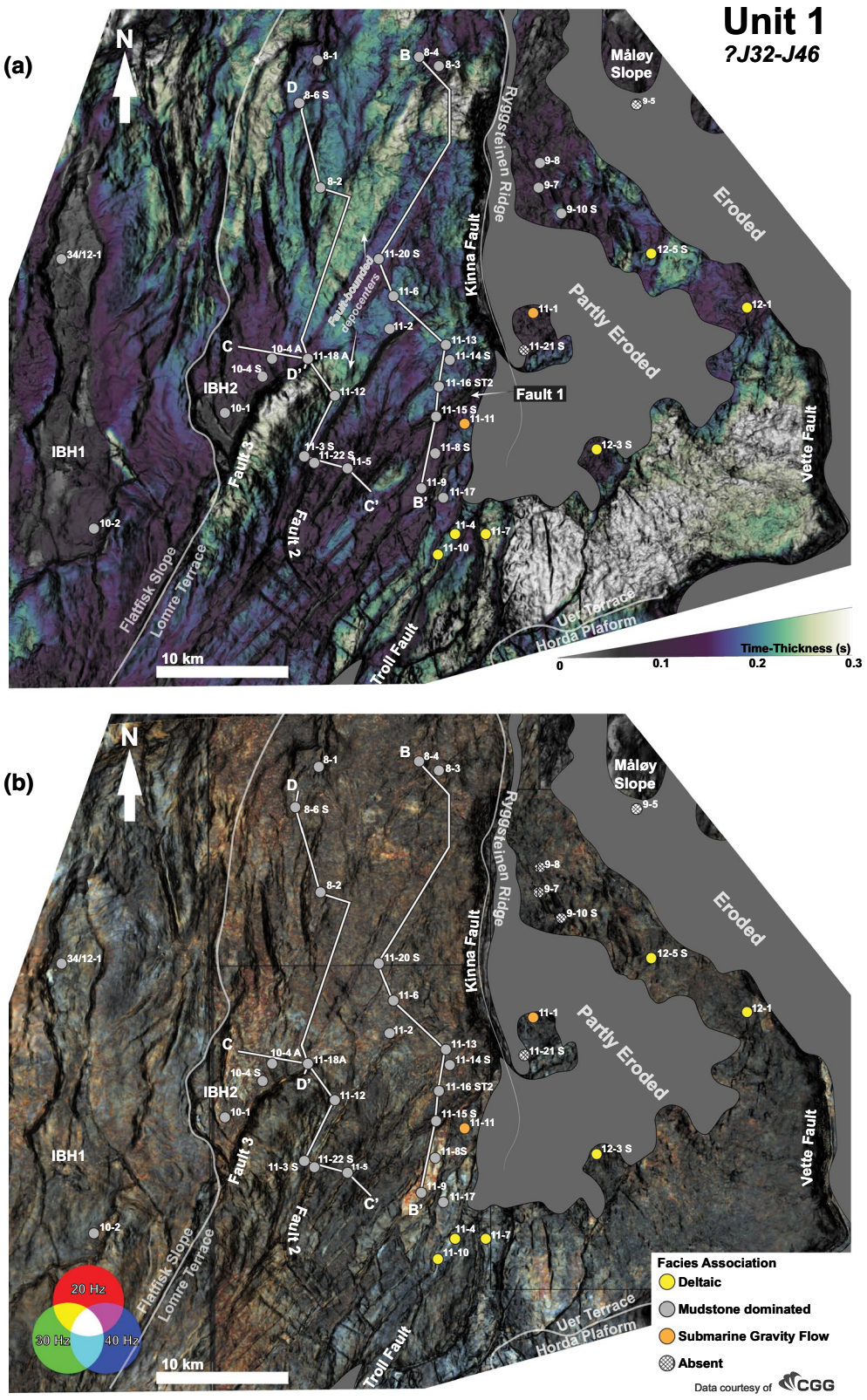

FIGURE 13 Seismic expression of SU1 (ca. Bathonian–late Callovian). (a) Time-thickness (Horizons 1–2) map with variance overlay. (b) Frequency decomposition RGB-blend with variance attribute overlay, red colour channel is 20 Hz, green colour channel is 30 Hz and blue colour channel is 40 Hz. Wells colour coded into simplified facies association interpretations

Lomre Terrace and Flatfisk Slope (Figure 13a). Strata on the Uer Terrace thicken towards the E/SE into the Vette Fault hanging wall. In contrast, SU1 does not show systematic thickening into the hanging wall of the Kinna Fault. Two fault-bounded intra-basin highs in the western part of the study area are capped by condensed SU1 (Figure 13, IBH

1&2). The Ryggsteinen Ridge and Måløy Slope are strongly eroded by younger composite unconformities (Jackson et al., 2008), which makes palaeogeographical reconstructions challenging.

Seismic Unit 1 is dominated by SF6 and lacks clear geomorphological elements (Figure 13b). Wells from the Lomre Terrace penetrating this interval consistently contain mudstone strata with only a minority of wells encountering coarse-grained sediments on the terraces within SU1 (35/11-11 and 35/11-1, Figure 13). Vertical smearing of the high amplitudes from sandstones in younger, overlying seismic units causes the high-amplitude events around wells 35/11-9 (Figure 13b). Sandstone-rich gravity-flow deposits proven in wells 35/11-1 and 35/11-11 on the NE Lomre Terrace and the southern Ryggsteinen Ridge do not have a distinct seismic geomorphological signature in contrast to the surrounding mudstone strata. Wells 35/11-4, -10, -7 in the E Lomre Terrace and 35/12-1, -3S on the NW Uer Terrace contain thick Krossfjord and Fensfjord Formation sequences. The proximity of the Uer Terrace to the basin margin and the Horda Platform, together with the high thickness values, suggests that the deposits represent the northern extension of the deltaic sequences dominating the Horda Platform. Although sand rich, these deltas were never able to supply substantial amounts of sand to the slope during the Bajocian–Callovian.

8.2 | Seismic Unit 2 (early Oxfordian–mid Oxfordian; J46–J54)

This unit is bound by Horizons 2 and 3, and is of early Oxfordian to mid Oxfordian age. Incisions associated with overlying SF4 and SF5 canyons in the footwall of the Kinna Fault (Ryggsteinen Ridge) and the terraces locally removed some SU2 stratigraphy. Maximum thickness reaches 0.2 s (TWT) in the hanging wall of the N-S-striking Kinna Fault and northern Lomre Terrace (Figure 14a) and overall, strata thin westward to time-thickness of <0.06 s (TWT) on the Flatfisk Slope, where SU2 has a relatively uniform thickness.

The NE-trending depocenters in SU1 on the Lomre Terrace continue to show across-fault thickness variations in SU2, especially along Fault 1, and the northern parts of faults 2 and 3 (Figure 14a).

Thickening towards the Kinna Fault suggests that it became active during the early to mid Oxfordian time and that previously active NE-SW-striking faults remained active from the Callovian until the mid Oxfordian. Remnants of early-to-mid Oxfordian sediments on the Ryggsteinen Ridge are proven by wells 35/11-1 and -21S, as well as in 35/9-8, -7 and -10S (Koch et al., 2017). This suggests that, even though the Kinna Fault was active, the Ryggsteinen Ridge was not emergent at this time and that deposition occurred in both its footwall and hanging wall.

The frequency decomposition blend for SU2 is higher amplitude overall compared to SU1 (Figure 14b). High amplitudes in all frequency bands are observable on the Lomre Terrace (e.g. in Fault 3 hanging wall), the western part of the Kinna Fault hanging wall and on the Flatfisk Slope. These areas can be linked to thin (<20 m) gravity flow sandstones in wells 35/11-3S, -12, 18A (Figure 12b), 35/11-6, -20S (Figure 12a) and 35/8-2, -6S (Figure 12c). The correlation between westward thinning and brightening of SU2 could be caused by tuning. The depositional thick area in the immediate hanging wall of Kinna Fault and Fault 1 shows a low-amplitude character, even though wells in this area penetrate turbidite sandstone in wells 35/11-13, -16 ST2 or -15S (Figure 12a) (Bakke et al., 2013). Gravity flow sandstones in the northernmost Kinna Fault hanging wall wells 35/8-4 and -3 (Ravnås et al., 2000) are also located in an area of very low amplitude, however, channelization and amalgamated, patchy to lobate shapes of Seismic Facies 1 (*Channelized Lobes*) can be defined (Figure 14c). Channel geometries are 0.5–1 km wide and have moderate sinuosity, whereas lobes range in width from 1 to 5 km (Figure 14c). The well 35/11-13 and surrounding wells penetrate >100 m of sand-rich gravity flow deposits, calibrating the lithology for the observed lobes and channels (Figure 12a/Figure 14c) (Bakke et al., 2013).

High amplitudes in the hanging walls of E-dipping faults 2 and 3 on the Lomre Terrace comprise fault-confined turbidite sheets (SF2). Wells on the footwall of E-dipping of Faults 2 and 3 (Figure 12b) show thin layers of gravity-flow sandstone, suggesting potentially thicker deposits in adjacent hanging wall growth wedges. The Flatfisk Slope contains 1–1.5 km wide gravity flow channels (SF3) with higher amplitudes compared to those on the Lomre Terrace but with dimmed amplitudes in the westernmost part of the study area leading into the North Viking Graben. The channels are dominantly fault transverse, except in the NW most area, where an intra-basin high deflects the channels into a northerly orientation (IBH 1, Figure 14). We hypothesize that the change from the SF4 channelized lobe complex in the hanging wall of the Kinna Fault to low sinuosity channels on the down-dip Flatfisk Slope could indicate an increased palaeoslope on the Flatfisk Slope. However, without direct age constraints by well data on the Flatfisk Slope, the exact age of these features is uncertain. In the eastern part of the study area, including Uer Terrace, Ryggsteinen Ridge and Måløy Slope, wells consistently report early-to-mid Oxfordian gravity flow deposits (Koch et al., 2017), but severe younger erosion of

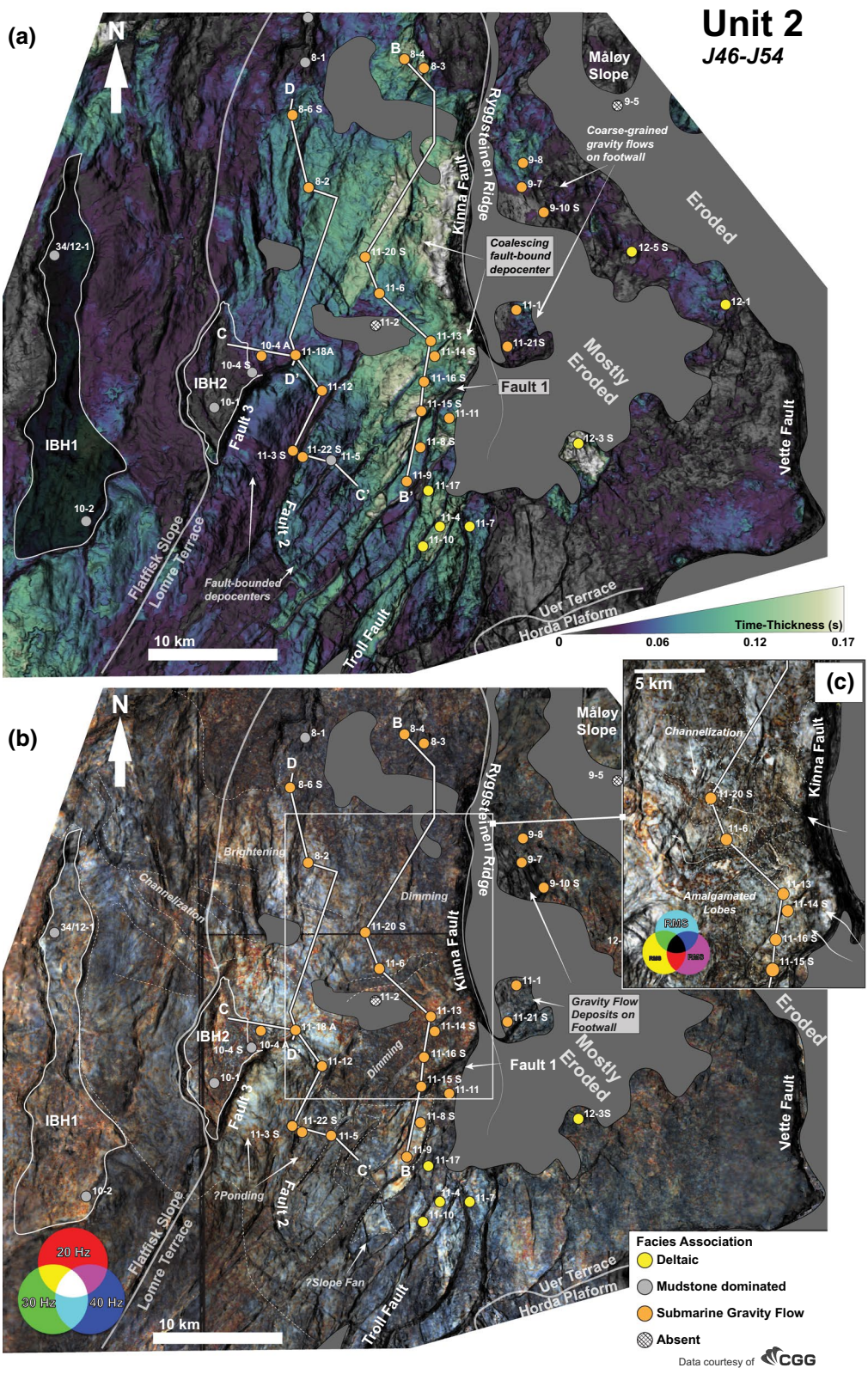

FIGURE 14 Seismic expression of SU2 (ca. early Oxfordian–mid Oxfordian). (a) Time-thickness (Horizons 2–3) map with variance overlay. (b) Frequency decomposition RGB-blend with variance attribute overlay, red colour channel is 20 Hz, green colour channel is 30 Hz and blue colour channel is 40 Hz. Wells colour coded into simplified facies association interpretations. (c) Exchroma (RMS-windowed) CMY blend with variance overlay of the dim stratigraphy in the hanging walls of Fault 1 and Kinna Fault, yellow colour channel is narrow RMS window (2 ms), magenta is moderate RMS window (4 ms) and cyan is wide RMS window (6 ms)

this area precludes detailed interpretation of SU2 seismic geomorphology.

Thickness maps and seismic geomorphology variations do not converge into common updip entry points, suggesting a line-source slope setting in SU2. The key driver for the vast supply of shelf-derived sediments to the deep-water terraces may have been at least two periods of relative sea-level fall in the early and mid Oxfordian (3-series, Dreyer et al., 2005; Patruno et al., 2015). For example, time-equivalent stratigraphy on the Horda Platform records a shift from fully marine to brackish conditions, marked progradational facies and seismically resolvable incision (up to 40 m deep) in the mid-early Oxfordian (Dreyer et al., 2005). A second major regression is also proposed for the mid Oxfordian, depicted by a significant basinward shift of facies in cores and marked incision on the Horda Platform (Dreyer et al., 2005).

8.3 | Seismic Unit 3 (late Oxfordian–early Kimmeridgian; J54–J62)

Seismic Unit 3 is bounded by Horizons 3 and 4 and is thinner than SU2 (typically <0.08 s TWT or ca. 130 m), and in many parts of the study area close to tuning thickness. Furthermore, it is severely affected by younger erosion, particularly in the E of the study area, complicating reconstruction of its palaeogeography. The main depocenters of SU3 are on the northern Lomre Terrace, and in particular the hanging walls of Faults 1–3 (Figures 12a/b and 15a). Faults 1 and 2 bound a depocenter with the greatest thickness for this unit. A distinct, fault-bound depocenter also occurs in the hanging wall of Fault 3, whereas the northernmost ca. 5 km of Fault 1 show isochronous strata in its footwall and hanging wall suggesting the N tip of Fault 1 was blind. The Kinna Fault hanging wall exhibits thickness variations between 0.06 and 0.08 s (TWT) (ca. 100–130 m) and suffers incision from overlying, younger submarine canyons, which have removed most of the late Oxfordian–early Kimmeridgian (Figures 12a/c and 15a). This makes it difficult to identify growth strata along the Kinna Fault hanging wall, however, preserved deposits in the central Kinna Fault hanging wall do not show distinct thickening towards the fault, suggesting limited fault activity during SU3.

The overall amplitude character of SU3 is comparable to SU2, but areas with bright responses in all frequency bands are less extensive (Figure 15b). High-amplitude areas that well data prove contain gravity flow sandstone (e.g. 35/11-12, -5, -18A) and *Submarine Channel Belt* seismic facies (SF3) are more confined compared to SU2 and occur only on the northern Lomre Terrace and the southern Kinna Fault hanging wall. Well 35/11-20S is located within a dimmed distributary channel and does not contain coarse-grained sediment within this interval (Figures 12a and 15b). In contrast, wells within high-amplitude anomalies surrounding the dimmed channel (e.g. 35/11-6) contain coarse-grained gravity flow deposits (cf. Figure 12a/c). This correlation suggests that dimmed channels in SU3 are likely mudstone-filled, whereas high-amplitude channels and sheets likely contain sandstone-dominated deposits. The northern Kinna Fault hanging wall is again relatively low amplitude, as in SU2, but wells penetrating SU3 contain mudstones.

On the central Lomre Terrace numerous 0.5–1 km wide SF3 distributary channels occur within the fault-bound isochron thick and fan out into sheet-like amplitudes in the immediate hanging wall of E-dipping Fault 2 (Figure 15b). Channels located at the northern tip of Fault 2 do not show signs of significant deflection due to fault topography and extend north-westward across the northern hanging wall of Fault 3 and into its footwall. In contrast, further S in the centre of Fault 2, high amplitudes terminate sharply against the fault and its footwall is dimmed (Figure 15b). Well 35/11-3S in the immediate footwall of Fault 2 (Figure 12b) confirms the absence of coarse-grained deposits.

The shift of the main depocenters from the immediate hangingwall of the Kinna Fault (SU2; Figure 14a) to the northern Lomre Terrace and hanging wall of Fault 2 with pronounced eastward thinning (SU3; Figure 15a) indicates compensational stacking of depocenters during SU3. We further suggest that the deep-water sedimentary systems of SU3 show stronger fault control than in SU2. As exemplified by central and SW parts of Fault 2, fault-related topography is sufficient to potentially block gravity flows (Figure 15b). Areas towards fault tips potentially allow for gravity flow systems to cross faults topography, as exemplified by NE parts of Fault 2 (Figure 15b). The NW-SE oriented submarine channel belt (SF3) in SU3 seems to converge into the relay zone between Kinna and Troll Fault, where previous palaeogeographical interpretations have proposed a prograding subaerial delta front extending out from the northern Horda Platform (Dreyer et al., 2005; Patruno et al., 2015). Seismic Unit 3 is the time of maximum progradation of the Sognefjord delta (approx. Top 5 series, Dreyer et al., 2005; Stewart et al., 1995). This narrowing between shelf break and delta plain parallels characteristics of shelf-edge deltas (Galloway, 1998; Muto & Steel, 2002), or at least it provided an abundance of coarse-grained gravity flows derived from river plumes to the terraces in SU3 (Hizzett et al., 2018; Piper & Normark, 2009; Plink-Björklund & Steel, 2004).

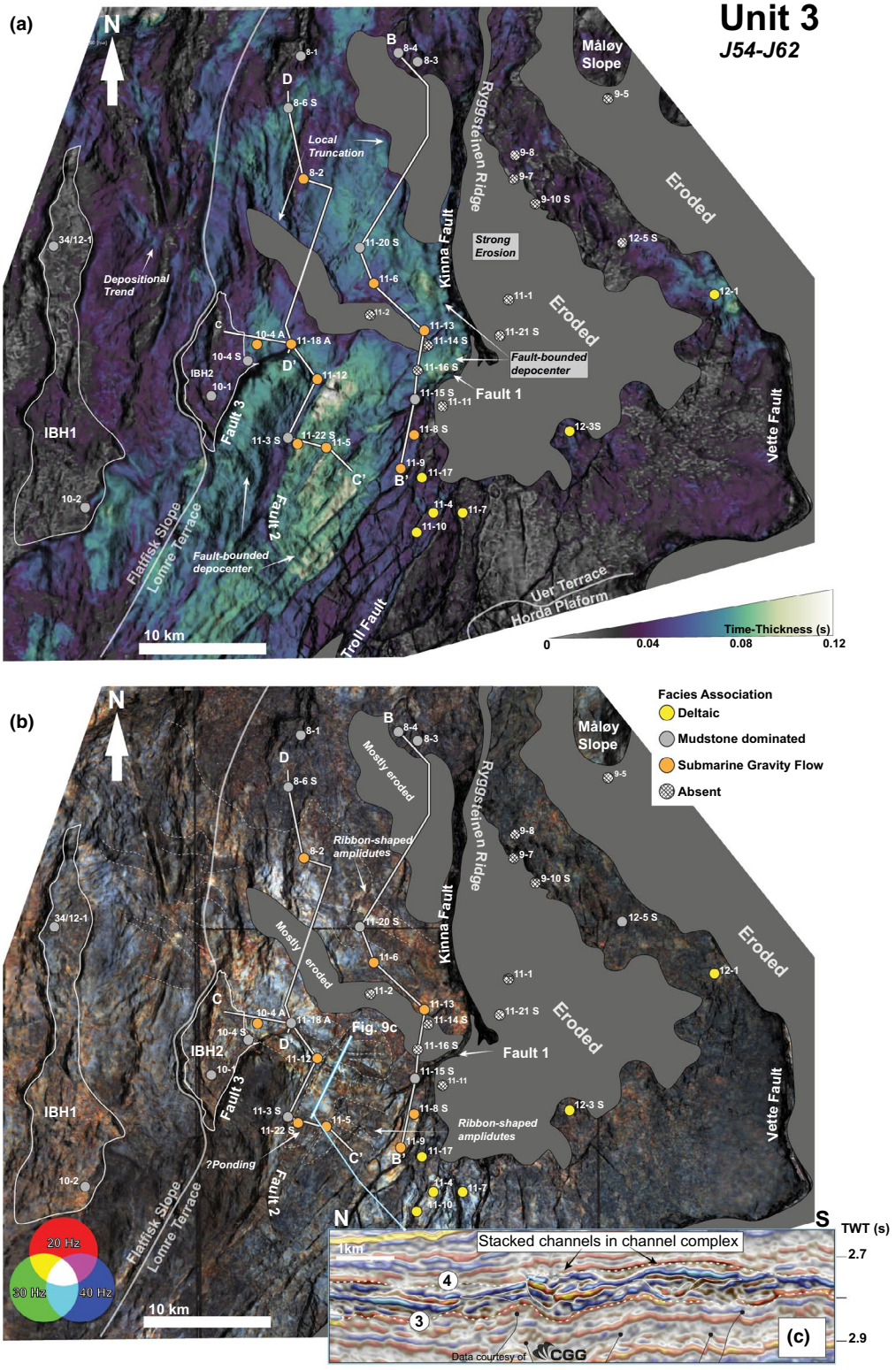

FIGURE 15 Seismic expression of SU3 (ca. mid Oxfordian–late Oxfordian). (a) Time-thickness (Horizons 3–4) map with variance overlay. (b) Frequency decomposition RGB-blend with variance attribute overlay, red colour channel is 20 Hz, green colour channel is 30 Hz and blue colour channel is 40 Hz. Wells colour coded into simplified facies association interpretations. (c) Seismic section through the hanging wall of antithetic (SE-dipping) Fault 2, orthogonal to the interpreted gravity flow fairway routing direction

8.4 | Seismic Unit 4 (early Kimmeridgian–latest Kimmeridgian; J62–J64)

Seismic Unit 4 is bounded below by Horizon 4 and above by Horizon 5. Horizon 4 is characterized by major SF4-related canyon incision to the E of the Kinna Fault that deeply erodes into the previous syn-rift seismic units along the canyon axis (Figure 16). West of the Kinna Fault, the down-flow continuation of the deeply incised canyons are more subtle, with limited incision associated with distal submarine canyon seismic facies (SF5) (Figure 16). Previous work on the Måløy Slope has suggested canyon incision to be initiated in the early Kimmeridgian times (Jackson et al., 2008; Reeve et al., 2015).

SU4 is absent in the two available wells on the Uer Terrace (35/12-1, -3S). Seismic mapping did not show a significant increase in thickness away from the well position, which suggests that SU4 thickness E of the canyons is below seismic resolution and the area characterized by non-deposition during SU4 times. Figure 16a, thus, shows a composite thickness map E and W of the Kinna Fault. The Uer Terrace shows three NE-SW-trending, ca. 5- to 10-km-wide dendritic canyon heads (Canyon 1, 2 and 3; Figure 16) that consist of five, 2- to 3-km-wide tributaries. Two tributaries merge into Canyon 1 at the southern tip of the Kinna Fault and pass into distal submarine canyon seismic facies (SF5) on the Lomre Terrace. To the N of Canyon 1, on the Uer Terrace, three tributaries merge into Canyon 2 that crosses the Ryggsteinen Ridge in a NW direction and passes into distal canyon seismic facies on the northern hanging wall of the Kinna Fault (Figure 16). Canyon 3 is located on the Måløy Slope, N of the Canyon 2. Canyon axis incision shows almost complete removal of underlying Late Jurassic deposits in more proximal locations (Figure 16a). Due to the lack of well penetrations within the canyons, the presence of SU4 deposits in the proximal canyons cannot be proven. In the distal parts of the canyons W of the Kinna Fault, subtle thickness variations within the canyons are mappable (Figure 16a), however, the exact onlap location of SU4 strata onto the proximal canyon base cannot be clearly mapped across the Kinna Fault.

In the hanging wall of the Kinna Fault, thicknesses are typically below 0.08 s TWT (Figure 16). Prominent features are two NE-SW- to NNE-SSW-trending thins that are the down-dip continuations of the proximal submarine canyons in the footwall of the Kinna Fault (Figure 16a). The depth of canyon incision on the Lomre Terrace and hanging wall of the Kinna Fault is significantly lower and usually <0.05 s (TWT), compared to canyon incisions depth often exceeding >0.2 s (TWT) in the footwall of the Kinna Fault (cf. SF4 and SF5; Table 2). This suggests that the distal courses of Canyon 1 and 2 W of the Kinna Fault have been more prone to sediment bypass during SU4 times and gravity flows less erosive than in proximal canyon locations. Areas outside of the canyons on Lomre Terrace and hanging wall of the Kinna Fault are between 0.03 and 0.08 s (TWT) thick and mud-dominated (Figure 16a). We suggest that they represent overbank deposits derived from unconfined low-density turbidity currents or hemipelagic fallout in areas not affected by canyon erosion or gravity flow bypass. Most of the aggradation within the canyons happened during SU5 by mud-prone backfill (Figure 10).

Up-dip areas in SU4, E of the Kinna Fault show a relatively uniform low frequency dominated response within, as well as outside of the canyons (Figure 16b). Areas N of the confluence of Canyon 2 tributaries between well 35/12-5S and 35/9-10S show channel-like features with a broadly SSE-NNW orientation. Some wells in the footwall of the Kinna Fault (35/9-7, -8; Figure 16b) are located to the N outside the axis of Canyon 2 and prove thin Kimmeridgian gravity flow deposits. These could have derived from Canyon 2, either by overbank deposition, or due to canyon deflection as response to uplift and backtilting on the immediate footwall of the Kinna Fault and associated abandonment of distal parts of Canyon 2 in the hanging wall of the Kinna Fault (Figure 16c).

West of the Kinna Fault, on the Lomre Terrace, the Flatfisk Slope and the hanging wall of the Kinna Fault, amplitudes are highly dimmed in all frequency bands outside of the canyon pathways (Figure 16b). Higher amplitudes in the canyon are dominantly within low frequencies and appear in reddish colours. Exceptions are the intrabasinal elevations (IBH1 and 2) and within Canyon 1 on the northern Lomre Terrace, which have a high amplitude in all frequency bands (Figure 16b). Wells near the amplitude anomalies within Canyon 1 (e.g. 35/11-2, -13; Figures 12 and 16b) confirm thin gravity flow sandstones, whereas wells outside of the bright amplitude are dominated by high-gamma ray mudstone. Canyon 2 extends into the hanging wall of the Kinna Fault and lacks the bright amplitude anomaly of Canyon 1, but the exchroma CMY blend (Figure 16c) reveals internal sinuous geomorphology within the canyon. Canyons 1 and 2 extend for more than 30 km to the NW down the Flatfisk Slope towards the North Viking Graben.

8.5 | Seismic Unit 5 (early Tithonian–late Tithonian; J64–J74)

Seismic Unit 5 is bound by Horizons 5 and 6. The time-thickness map is relatively isochronous over large parts of the study area. Larger, 0.2–0.3 s TWT thick, coalesced syntectonic depocenters are identified along the hanging wall of the Kinna Fault, its relay to the Troll Fault, and in the

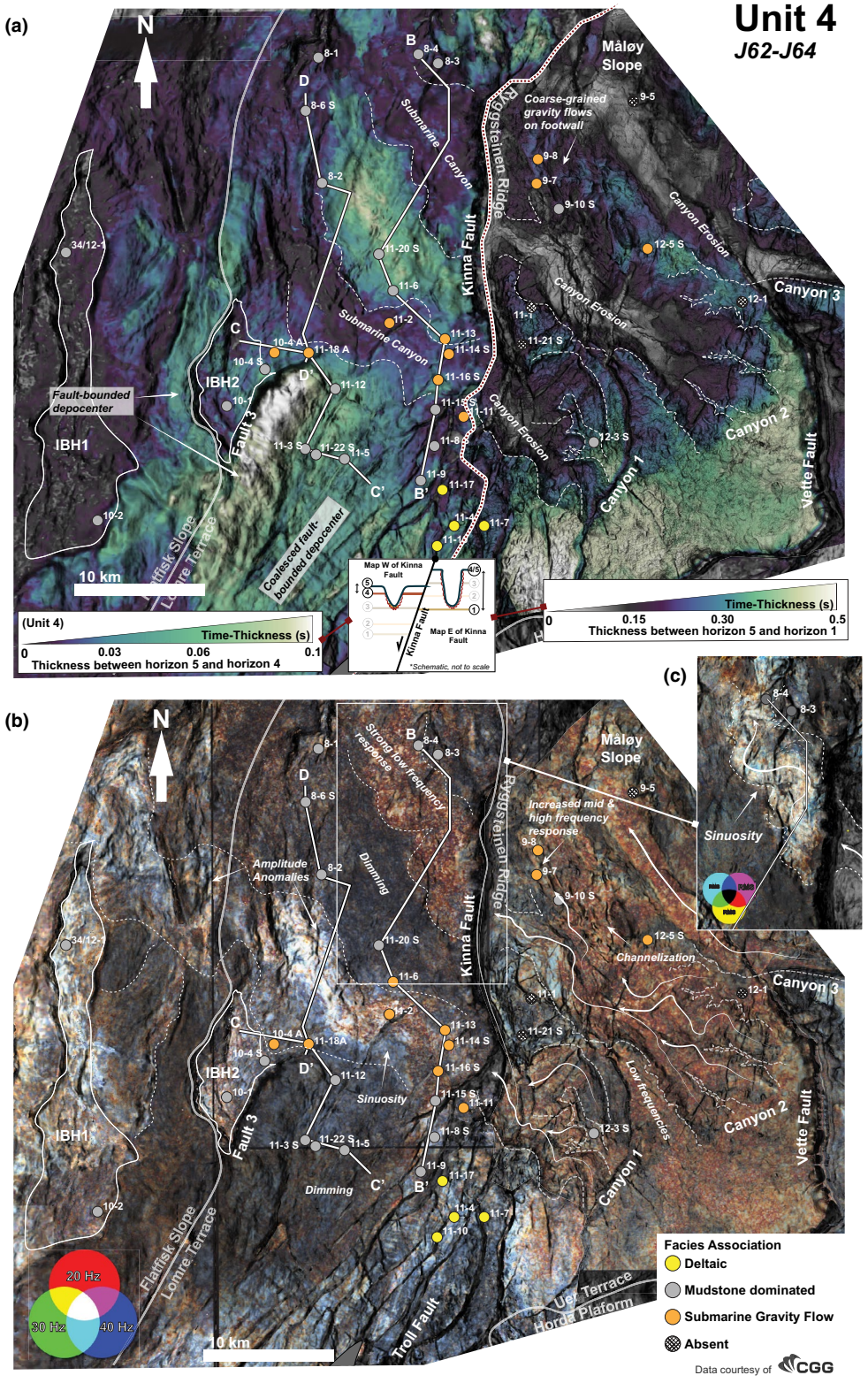

FIGURE 16 Seismic expression of SU4 (ca. early Kimmeridgian–late Kimmeridgian). (a) W of Kinna Fault: time-thickness map (Horizons 4–5) with variance overlay; E of Kinna Fault: time-thickness top SU4 – base syn-rift (Horizons 1–5). (b) Frequency decomposition RGB blend with variance attribute overlay, red colour channel is 20 Hz, green colour channel is 30 Hz and blue colour channel is 40 Hz. Wells colour coded into simplified facies association interpretations. (c) Exchroma (RMS windowed) CMY blend with variance overlay of submarine canyon 2 in the hanging wall of the Kinna Fault, yellow colour channel is narrow RMS window (2 ms), magenta is moderate RMS window (4 ms) and cyan is wide RMS window (6 ms)

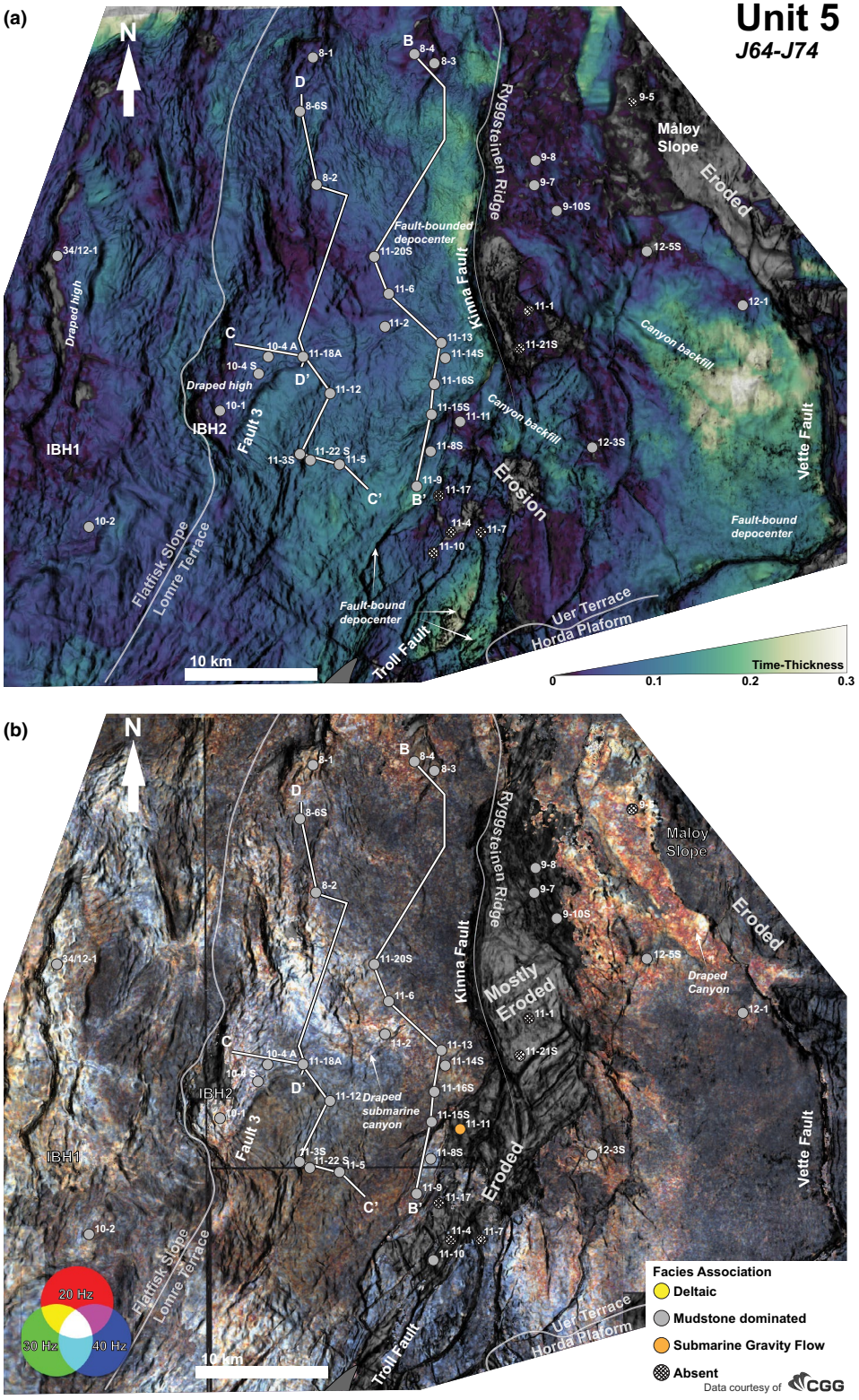

FIGURE 17 Seismic expression of SU5 (ca. early Tithonian-early Berriasian). (a) Time-thickness (Horizons 5–6) map with variance overlay. (b) Frequency decomposition RGB blend with Variance overlay, red colour channel is 20 Hz, green colour channel is 30 Hz and blue colour channel is 40 Hz. Wells colour coded into simplified facies association interpretations

hanging walls of intra-basin high 2 (IBH2) (Figure 17a). The Kinna Fault shows thinning to complete absence of SU5 in its footwall. This suggests crestal degradation and/or condensed strata on the footwall, indicating that the Ryggsteinen Ridge was a major intra-basinal elevation during this time. Seismic Unit 5 on the Uer Terrace thickens

towards the Vette Fault and is also thick within Canyon 2 (>0.3 s TWT, >500 m).

The frequency decomposition RGB blend (Figure 17b) extracted below Horizon 6 overall shows the SF6 seismic geomorphologic character within SU5. Some areas located above SU4 canyons appear as high-amplitude areas which mimic the canyon shape. This expression was interpreted to be largely caused by vertical smearing of the high-amplitude reflection of SU5 mudstone drape against the canyon base and potential gravity flow deposit fills. None of the wells penetrate coarse-grained deep-water deposits on the terraces. The uplifted eastern parts of the Horda Platform and the Ryggsteinen Ridge have been interpreted to have been footwall islands fringed by shoreface sands during a pronounced Tithonian sea-level lowstand (Fraser et al., 2003; Roberts et al., 2019). Coarse-grained sediment supply from the regional hinterland catchment ceased during SU5 as the Late Jurassic rift entered a phase of thermal cooling and a gradual rise of the relative sea level occurred throughout the late Tithonian (Fraser et al., 2003; Jackson et al., 2008).

9 | SYNTHESIS OF TECTONO-SEDIMENTARY EVOLUTION

We focus on the major gravity flow fairways in SU2, SU3 and SU4, which are interpreted to be sourced from rift-hinterland drainage systems during the Oxfordian to Kimmeridgian. The regressive periods (cf. Figure 2, *'Relative sea-level'* and *'Shoreline position'*) are separated by maximum flooding surfaces, as constrained by Partington, et al. (1993). The Horda Platform as up-dip staging area for the gravity flow fairways is considered to be relatively stable until SU4 times, which suggests that the deposition of associated shallow marine wedges is mostly supply driven (e.g. Dreyer et al., 2005). The increased fault activity on the Kinna Fault during SU4 is contemporaneous with basin-wide strain localization and the highest Late Jurassic extension rates (Færseth et al., 1997; Partington, Mitchener, et al., 1993; Ravnås et al., 2000; Stewart et al., 1995). The northern Horda Platform shows first signs of rotation and drainage reversal on the large 6- to 15-km-wide, E-dipping fault blocks during SU4 time, with dip-slope fans overlying the late Oxfordian prograding sequences (Dreyer et al., 2005; Whipp et al., 2014). Canyons 1, 2 and 3 are part of a regional unconformity complex with canyon features extending for more than 150 km along the basin margin to the N, which has been inferred to be caused by basinward tilting of the rift margin due to increased subsidence in the rift axis areas (Jackson et al., 2008, 2019; Koch et al., 2017; Sømme & Jackson, 2013; Sømme et al., 2013), which is likely amplified by high seasonal runoff rates during the humid Kimmeridgian climate (Armstrong et al., 2016). The following subsections will summarize generic observations from the Late Jurassic submarine gravity flow deposits on the Lomre and Uer terraces, with focus on sediment routing and depositional architecture throughout the rift phase.

9.1 | Normal faulting and sediment routing

The structural framework of the terraces evolved from distributed faulting in the early syn-rift phase (SU1–SU3; Bathonian–late Oxfordian) to localized faulting on fewer large normal faults in the later syn-rift phase (SU4–SU5; early Kimmeridgian–late Tithonian). The progressive localization of strain onto the Kinna Fault, Fault 1 and Fault 3 results in larger, amalgamated depocenters with decreasing internal segmentation and more pronounced across fault topography. Mirroring the structural evolution, the gravity flow systems became increasingly confined, suggesting increasing fault topography focused the depositional systems through relay zones between fault segments. The gravity flow systems are dominantly oriented rift transverse, largely orthogonal to the fault strike, and follow the regional gradient towards the NW into the rift axis graben (Figure 3, NVG).

Seismic Unit 2 is deposited during ca. 3.5 Myr and is characterized by the most widespread gravity flow deposition (Figures 14 and 18b). Most of the normal faults appear active during SU2 and show syn-kinematic strata in their hanging walls. During SU3 (ca. 2-2 Myr.) normal faulting became more localized onto fewer structures (e.g. Faults 1–3 and the Kinna Fault; Figure 15a) and the gravity flow fairway becomes more confined into a narrow corridor on the N Lomre Terrace and S hanging wall of the Kinna Fault, which contains larger, aggradational submarine channels (Figures 15c and 18c). In SU4, which spans 4 Myr, the trend of confinement continues with the formation of submarine canyon systems. Normal faulting is localized on the Kinna Fault and Fault 3 with few other faults active (Figure 16a/Figure 18d). The seismic geomorphology (Figure 16b/Figure 18d) suggests fault-related topography was sufficient to deflect some of the canyon systems (e.g. Canyons 2 and 3), leading to abandonment of the previous canyon routing across the hanging wall of the Kinna Fault and re-direction onto the Ryggsteinen Ridge (Figure 16b). In contrast, Canyon 1 is located within a relay zone and shows no significant deflection. Figure 18d depicts both sub-periods in SU4, an initial period where Canyon 2 extends across the Kinna Fault, and a later period when gravity flows were deflected northward.

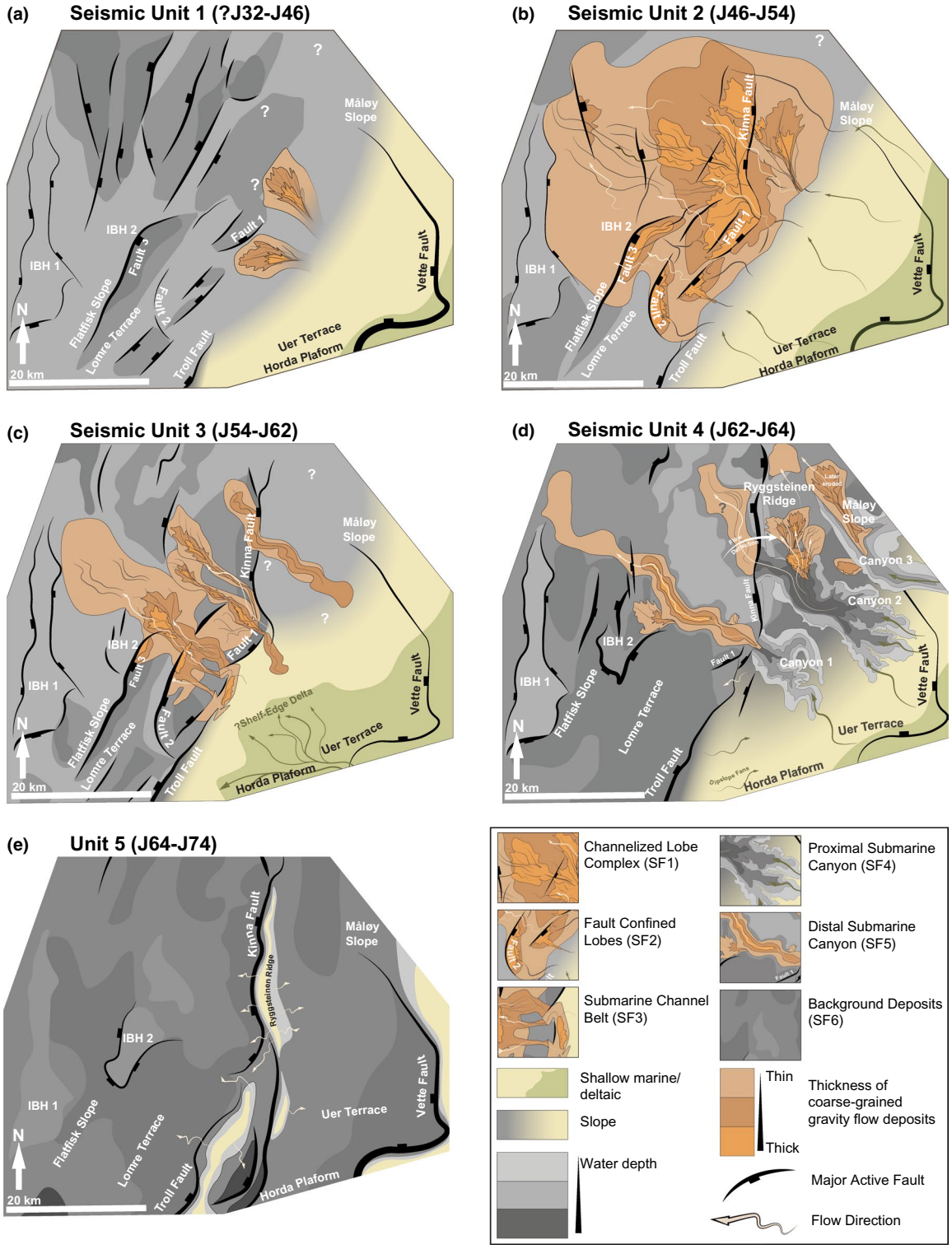

FIGURE 18 Simplified line drawing of the sedimentary systems on the fault terraces and the evolution of the gravity flow fairway throughout the Late Jurassic. Major faults are illustrated for orientation, however, activity is not limited to depicted faults. Numerous smaller faults were active and may have significant impact on gravity flow deposition on a local scale. Depth scale: shallow (light grey) to deep (dark grey), coarse-grained deep-marine clastics: thick (orange) to thin (pale orange)

9.2 | Gravity flow depositional architecture

Within each of the seismic units, we interpreted a range of depositional architectures and local interactions between normal faults and gravity flow lobes or channels. In the first seismic sequence with significant syn-rift gravity flow deposit (SU2), the depositional architecture is characterized by patchy lobes within a large channelized lobe complex

(Figure 18b). Thickest deposits are located in the immediate hanging wall of the Kinna Fault (Figure 14b/Figure 18b). The channelized lobe complex is sand rich, mostly amalgamated and relatively massive (>100 m thick). Transport further downdip is suggested by incision of younger channels into the lobe complex. Further S, in westward rotated half-graben bound by Faults 2 and 3, ponding of gravity flows is interpreted at fault-segment centres for SU2 and SU3 (Figure 18b/c). In both seismic units, gravity flow depositional systems do not appear to have been completely blocked by fault topography, but 'partially ponded' (cf. Shultz & Hubbard, 2005) in their hanging wall. As such, we do not envision a fill-and-spill scenario (Prather et al., 1998) for partially ponded gravity flows, but rather unconfined turbidity currents overriding faulted topography and being stripped off their basal, coarse-grained sediment load by emerging at-seafloor structures. In SU4, canyon formation is the dominant depositional style in the study area (Figure 18d). Associated, relatively thin gravity flow deposits are found next to or within the submarine canyons, which indicates that coarse-grained gravity flows were routed through these canyons. However, the overall small amounts of SU4 sandstone within the study area do not allow for a definition of seismically resolvable depositional architectures. Larger depositional lobes containing coarse-grained gravity flow deposits at more distal canyon locations in the rift axis cannot be ruled out.

10 | DISCUSSION – IMPLICATIONS FOR SEDIMENTATION IN DEEP-WATER RIFT BASINS

In the following section, we use the results from our analysis of the tectono-sedimentology of the Late Jurassic on the Lomre and Uer Terraces to discuss: (i) hinterland versus local footwall sediment sources for deep-water rift systems, (ii) deep-water sediment routing across down-stepping fault terraces and (iii) influence of fault geometry and evolution on deep-water gravity flow deposits.

10.1 | Hinterland versus local footwall sources for deep-water rift systems

Some syn-rift tectono-sedimentary models propose that sediment supply to deep-water sinks is predominantly locally derived from uplifted intra-basin footwall topography, either from the steep footwall scarp or down the gentler hanging wall dipslope (e.g. Gawthorpe & Leeder, 2000). However, several studies of active rift basins have suggested that major hinterland-sourced sediment routing systems are important for the development of gravity flows in rifts. Examples of hinterland drainage sourcing major syn-rift gravity flow depositional systems include the Gulf of Suez (e.g. Pivnik et al., 2003), the Gulf of Corinth (Cullen et al., 2019; Ford et al., 2017; Gawthorpe et al., 2018; Muravchik et al., 2019) and the East African Rift System (Scholz et al., 1990; Zhang & Scholz, 2015; Zhang et al., 2014). Our observations from the eastern flank of the Northern Viking Graben further highlight the importance of major hinterland drainage as sources for volumetrically significant syn-rift gravity flow systems. Furthermore, we did not observe any intra-basin footwall sediment sources that significantly contributed to the syn-rift gravity flow fairway.

10.2 | Deep-water sediment routing across down-stepping fault terraces

Axial systems that transport sediments along strike of individual rift basins are often invoked as key driver for sediment routing in the distal locations of deep-water rift basins (Gawthorpe & Leeder, 2000; McArthur et al., 2016; Ravnås & Steel, 1998). Relay ramps are further recognized as important conduits linking individual deep-water depocenters (Athmer et al., 2010; Ravnås & Steel, 1998). These geometries accurately capture rift physiography within major rift segments characterized by large normal faults and crustal-scale tilted fault-blocks. However, the results of this study suggest that in areas of distributed normal faulting, characterized by closely spaced fault terraces, deep-water sediment routing is different. The dominating sediment transport direction of the depositional fairways in SU2-SU4 is overall fault transverse, overriding the NE-SW fault strike, and following the overall regional north-western slope off the Horda Platform and into the North Viking Graben. Exceptions to transverse sediment routing are Canyons 2 and 3 in SU4, where the Ryggsteinen Ridge evolved as major intra-basinal high. The canyons are forced into a fault-parallel direction in the later stages of SU4 due to growth of the Kinna Fault and uplift and back-tilting of the Ryggsteinen Ridge (Figures 18d and 19b). In contrast, Canyon 1 in the relay zone between Troll and Kinna Fault maintains its fault transverse course (Figure 19b, B).

From SU1 to the early stages of SU4 the rift-induced strain is accommodated by a distributed array of small faults that, individually, produced only minor modifications to the regional slope from rift margin platform to rift axis basin floor. Thus, it is the regional slope gradient that is the dominant control on routing of deep-water depositional systems rather than the local fault-block topography associated with tilting and crestal uplift. Furthermore, the local fault-related topography on the terraces did not cause sustainable fault parallel diversion on the sedimentary fairway scale.

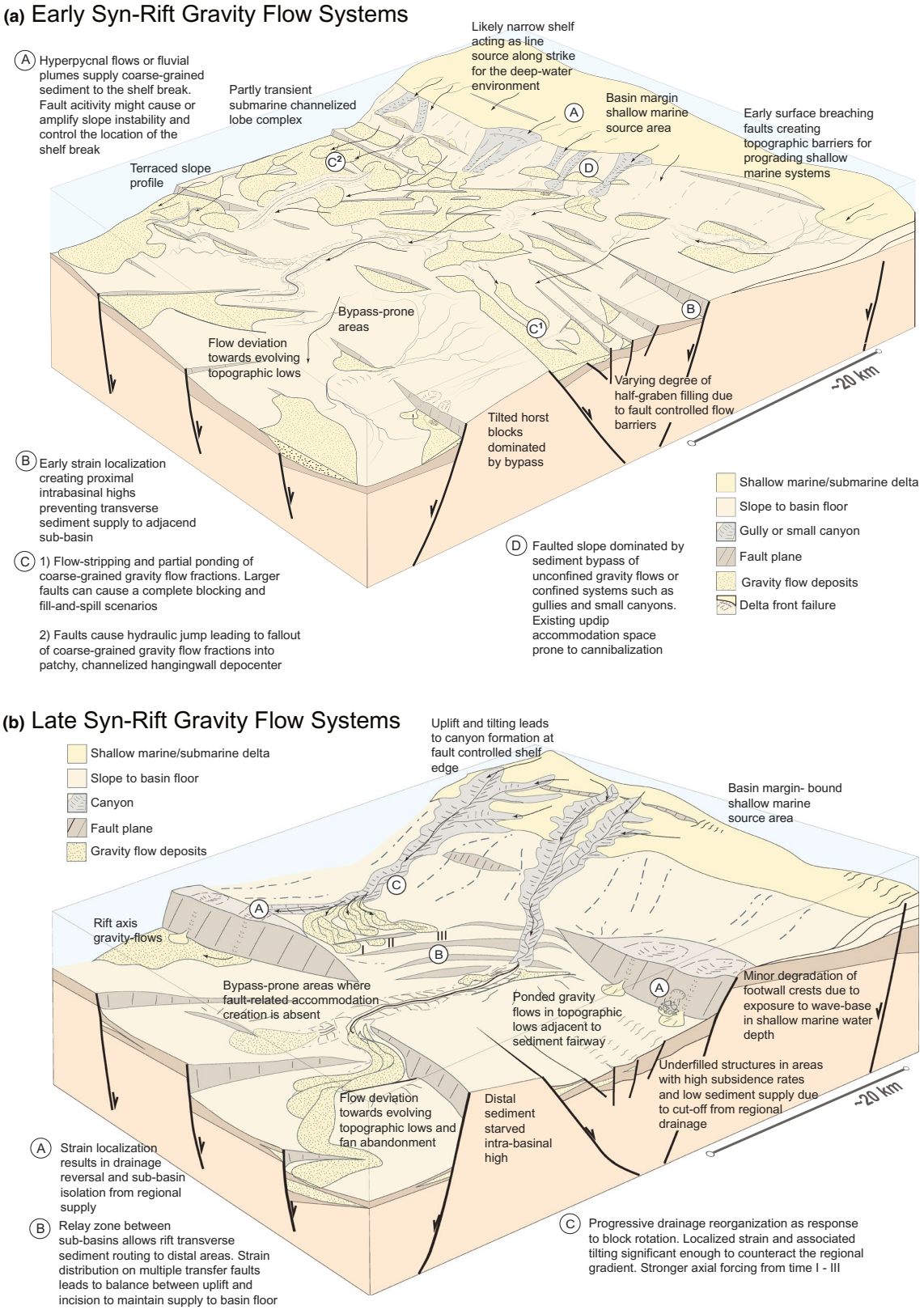

FIGURE 19 End-member type block models of syn-rift deep-water depositional systems in areas with distributed strain on faulted slopes or tectonic terraces and shallow marine sediment sources with regional hinterland drainage. (a) Early syn-rift stage. (b) Late syn-rift stage

The general trend of strain localization and coalescence of individual depocenters into large, linked sub-basins throughout the rift phase is common for most rifts (Cowie et al., 2000; Gawthorpe & Leeder, 2000). Concomitant with increasing localization of faulting and topography generation is a trend of increasing confinement of the deep-water depositional systems. This is illustrated by the gravity flow systems evolving from a line-sourced channelized lobe complex with limited impact on sediment routing in SU2 (Figure 18b), to channelized gravity flow deposits in SU3 (Figure 18c) and confined submarine canyons in SU4 (Figure 18d). This suggests that the degree of strain localization is important in controlling deep-water sediment routing pathways across active rift topography, even in areas of closely spaced fault terraces.

In major rift segments characterized by crustal-scale half-graben (e.g. Gawthorpe & Leeder, 2000; Henstra et al., 2016; Muravchik et al., 2018; Prosser, 1993), fault-controlled topography will increasingly isolate across fault individual depocenters and lead to less connection from rift margin to rift axis. Gravity flow deposits likely deposit in short transverse fairways, or flow axially, parallel to fault strike as fault linkage leads to subsidence of along strike hanging wall transverse highs (Gawthorpe & Leeder, 2000; McArthur et al., 2016; Ravnås & Steel, 1998). Deposits from these axial systems are considered as more mature because of their distance of transport compared to transverse systems locally derived from degradation of uplifted footwall crests (e.g. Athmer & Luthi, 2011; Henstra et al., 2016; McArthur et al., 2016; Ravnås & Steel, 1998).

In areas of closely spaced faulted terraces, such as in this study, transverse gravity flow systems in areas of distributed strain, follow a routing pathway that is primarily controlled by the regional gradient as opposed to the local fault trend (Figure 18b–d). The depositional systems extend across a large number of fault terraces over a distance of tens of kilometres from shelf edge to rift axis (cf. Figures 14–16). As a result, these deep-water gravity flow systems have long transport pathways that contain mature deep-water deposits in their distal sinks. Parts of these systems may become dominantly axial due to progressive strain localization during later stages of rifting, as exemplified by Canyon 2 (Figure 18d), and share more of an analogy with existing deep-water syn-rift models (e.g. Gawthorpe & Leeder, 2000; Prosser, 1993; Ravnås & Steel, 1998).

10.3 | Local normal fault control on fault transverse deep-water depositional patterns

We have previously discussed the large-scale sediment routing from the basin margin sources to the deep-water rift axis sinks. In this section, we focus on the local impact of normal faulting on gravity flow depositional architecture. Basin floor 'rugosity' or changes in bathymetric gradient (Kneller et al., 1999; Posamentier & Kolla, 2003) controlling gravity flow depositional systems is well documented from non-rift settings (e.g. Clark & Cartwright, 2009; Deptuck et al., 2007; Mayall et al., 2006; McHargue et al., 2011). Comparable structural-gravity flow relationships are less well documented from rifts, with some exceptions (e.g. Adeogba et al., 2005; Cullen et al., 2019; Jackson et al., 2011; Kane et al., 2010).

Normal faults can be oriented parallel, orthogonal and oblique relative to the gravity flow direction. The end-member types with maximum fault interaction are where the gravity flows are oriented orthogonally to fault strike, and can either flow towards an up-slope dipping normal fault (antithetic relationship; Figure 19a, C1), or flow across the footwall of down-slope dipping normal faults to spill over into the hanging wall (synthetic relationship, Figure 19a, C2). Axial gravity flow systems, with flow direction parallel to the fault strike, are rare in our study.

Examples of the antithetic fault-gravity flow relationship are provided by Faults 2 and 3 in SU2 and SU3, which show topographic ponding of gravity flows in their half-graben (Figure 14b/Figure 15b). However, these examples do not suggest a complete blocking (sensu Clark & Cartwright, 2009) of deep-water systems. Contemporaneous gravity flow deposits are present in both hanging wall and footwall, suggesting sediment transport across the fault without significant deflection or diversion. This relationships suggest flow-stripping and partial ponding of the basal fractions of the gravity flow currents by 'antithetic' fault topography (cf. Shultz & Hubbard, 2005) is more likely, rather than a complete blocking and ponding of gravity flows in a fill-and-spill type evolution (sensu Prather et al., 1998). The diluted, lower-density fractions of the turbidity current can exhibit flow-thicknesses of more than 100 m (cf. Ge, Nemec, Gawthorpe, & Hansen, 2017; Ge, Nemec, Gawthorpe, Rotevatn, et al., 2017; Howlett et al., 2019), which suggests that at sea floor topography of several meters to 10s of meters will mostly affect the sand-laden basal parts of the current. This scenario is most dominant in early rift stages (Figure 19a), where normal fault networks show distributed strain and relatively small displacement on individual faults.

Examples of the synthetic fault-gravity flow relationship are provided by Fault 1 and the Kinna Fault (Figure 19, C2). The sudden gradient change from fault scarp to hanging wall causes a hydraulic jump within the gravity flow current that facilitates deposition of the coarse-grained fraction in the immediate hanging wall (Ge, Nemec, Gawthorpe, & Hansen, 2017). The depositional architecture observed in hanging walls of Fault 1 and the Kinna Fault show chaotic amalgamation of lobate and sheet-like character in SU2, which suggests a relatively rapid deposition from the gravity flows. Numerical modelling of interactions between gravity flows and such fault-controlled topography indicates that the resulting base of fault scarp fans have a more patchy spatial distribution of individual fan elements (Ge, Nemec, Gawthorpe, & Hansen, 2017; Ge, Nemec,

Gawthorpe, Rotevatn, et al., 2017), compared to existing slope fan models from non-rift settings with dominantly lobate geometries (e.g. Haughton et al., 2009; Prather, 2003; Reading & Richards, 1994; Richards et al., 1998). Comparable depositional styles have been interpreted on 3D seismic and well data of the Gudrun turbidite system in the South Viking Graben (Jackson et al., 2011) and syn-tectonic turbidite systems of the Niger Delta (Adeogba et al., 2005).

11 | SUMMARY AND CONCLUSIONS

We have summarized our observations from the Lomre and Uer terraces into a two-stage structural evolution model for syn-rift deep-water depositional systems on narrow fault terraced slopes. Figure 19a depicts the early stages of rifting, where deep-water sediments are sourced from a basin margin with hinterland drainage via shelfal, shallow marine depositional systems. Figure 19b illustrates more advanced stage of rifting, which is characterized by more localized faulting on few, large-scale terrace-bounding normal faults.

11.1 | Early syn-rift deep-water settings

- The gravity flow sediment routing follows the dominant regional slope gradient towards the deep rift axis graben and sediment is mostly sourced from basin-margin deltas or shelf edge failures (A and B; Figure 19a).
- The bathymetric relief is shaped by distributed faulting on numerous active normal faults. Prominent late stage faults may not have developed significant relief on the seafloor during this time. In cases of early localization of strain, rift transverse sediment routing may be diverted by larger fault related relief, leading to sediment starvation in the immediate hanging wall (B; Figure 19a).
- Sea-floor deformation by growing antithetic faults causes flow-stripping and partial ponding of coarse-grained fractions of the gravity flows. Larger antithetic normal faults can cause a complete blocking and ponding in their hanging wall (C^1; Figure 19a). The steep scarps and fault-related monoclines of synthetic normal faults promote hydraulic jumps in gravity flows that lead to deposition of coarse-grained fractions as patchy, channelized hanging wall deposits (C^2; Figure 19a).
- Updip depocenters on the fault terraced slope might become subject to cannibalization or bypass (D; Figure 19a) due to fault-related uplift. Vice versa, areas previously characterized by bypass or erosion might become depocenter due to fault-related subsidence.
- Gravity flow deposits generally wedge and thicken towards fault planes. However, depocenters are likely overfilled and limited seafloor differential relief across low-displacement normal faults allows for sediment accumulation on both footwall and hanging wall (C^1; Figure 19a).

11.2 | Late syn-rift deep-water settings

- The deformation focused on fewer, but large normal faults with increased hanging wall subsidence and footwall uplift rates, which creates greater seafloor rugosity across faults. Relay zones are localities where deformation remains distributed on numerous small-scale faults, which provides areas with less seafloor rugosity (A/B; Figure 19b).
- Many isolated depocenters are likely starved of coarse-grained sediments. Previously active gravity flow deposits in areas of localized faulting are abandoned and covered by hemipelagic drape. Footwall crests degrade and potentially become subaerially exposed as footwall islands.
- Submarine gravity flow depositional systems likely become routed through transfer zones due to the lower footwall relief compared to fault segment centres (B; Figure 19b). In contrast, transverse sediment routing across fault segment centres may be diverted due to footwall uplift and back-tilting (C; Figure 19b).
- Submarine canyons developed in the late rift stage, which provide effective rift-transverse sedimentary pathways linking basin margin and the deep rift axis graben over tens of kilometres. Large parts of the canyons may be bypass dominated and filled by mudstone following canyon abandonment.

Deep-water sediment routing follows the regional gradient towards the rift axis, largely unaffected by emerging at sea floor scarps and fault-block tilting, but with local fault topography influencing the depositional architecture of gravity flow deposits on a local scale. This contrasts most existing models of sedimentation in deep-water rift basins, focusing on settings with localized strain on major border faults and depositional style in the associated crustal-scale half-graben basins. Our results also emphasize the importance of regional hinterland-sourced basin-margin deltaic systems, as opposed to local fault crest degradation as primary control on the development of large, sand-prone deep-water syn-rift deposits.

ACKNOWLEDGEMENTS

This contribution forms part of the Syn-Rift Systems Project funded by the Research Council of Norway, Aker BP, ConocoPhillips, DNO, Equinor, Neptune and Tullow Oil (project number 255229) to the University of Bergen and academic partners at the universities of Leeds, East Anglia, Lorraine and the National and Kapodistrian University of Athens. We acknowledge Schlumberger for the academic software license of Petrel, Ellis for providing Paleoscan,

Cegal for providing the Blueback Reservoir Toolbox, and ffA for providing Geoteric. We thank CGG for providing access to their 3D seismic and well data for this study and NPD for access to the DISKOS database. We thank partners of the Syn-Rift Systems project and Tom Dreyer, Åshild Winsnes and Ranveig Halseth for insightful discussion about the study area. Finally, we thank the handling editor, Cari Johnson, and reviewers Ron Steel, Tiago M. Alves and anonymous reviewer 3 for their feedback, upon which the quality of the manuscript significantly improved.

PEER REVIEW

The peer review history for this article is available at https://publons.com/publon/10.1111/bre.12538.

DATA AVAILABILITY STATEMENT

The 3D seismic data that support the findings of this study are available from CGG Services Norway AS. Restrictions apply to the availability of these data, which were used under license for this study. Request to access to the seismic data can be made to CGG Services Norway AS. The well data are available from the Norwegian Petroleum Directorate via the DISKOS Database. The biostratigraphic data are available from CGG Services Norway AS and Equinor ASA. Restrictions apply to the availability of the biostratigraphic data, which were used under license for this study. A request for access can be made to CGG Services Norway AS and Equinor ASA.

ORCID

Fabian Tillmans https://orcid.org/0000-0003-1313-7973
Robert L. Gawthorpe https://orcid.org/0000-0002-4352-6366
Christopher A.-L. Jackson https://orcid.org/0000-0002-8592-9032
Atle Rotevatn https://orcid.org/0000-0002-8413-3294

REFERENCES

Adeogba, A. A., McHargue, T. R., & Graham, S. A. (2005). Transient fan architecture and depositional controls from near-surface 3-D seismic data, Niger Delta continental slope. *AAPG Bulletin*, *89*, 627–643. https://doi.org/10.1306/11200404025

Anders, M. H., & Schlische, R. W. (1994). Overlapping faults, intrabasin highs, and the growth of normal faults. *The Journal of Geology*, *102*, 165–179.

Anderson, J. E., Cartwright, J., Drysdall, S. J., & Vivian, N. (2000). Controls on turbidite sand deposition during gravity-driven extension of a passive margin: Examples from Miocene sediments in Block 4, Angola. *Marine and Petroleum Geology*, *17*, 1165–1203. https://doi.org/10.1016/s0264-8172(00)00059-3

Armstrong, H. A., Wagner, T., Herringshaw, L. G., Farnsworth, A. J., Lunt, D. J., Harland, M., Imber, J., Loptson, C., & Atar, E. F. L. (2016). Hadley circulation and precipitation changes controlling black shale deposition in the Late Jurassic Boreal Seaway. *Paleoceanography*, *31*, 1041–1053.

Athmer, W., Groenenberg, R. M., Luthi, S. M., Donselaar, M. E., Sokoutis, D., & Willingshofer, E. (2010). Relay ramps as pathways for turbidity currents: A study combining analogue sandbox experiments and numerical flow simulations. *Sedimentology*, *57*, 806–823.

Athmer, W., & Luthi, S. M. (2011). The effect of relay ramps on sediment routes and deposition: A review. *Sedimentary Geology*, *242*, 1–17.

Badley, M., Price, J., Dahl, C. R., & Agdestein, T. (1988). The structural evolution of the northern Viking Graben and its bearing upon extensional modes of basin formation. *Journal of the Geological Society*, *145*, 455–472.

Bakke, K., Kane, I. A., Martinsen, O. J., Petersen, S. A., Johansen, T. A., Hustoft, S., Jacobsen, F. H., & Groth, A. (2013). Seismic modeling in the analysis of deep-water sandstone termination styles. *AAPG Bulletin*, *97*, 1395–1419. https://doi.org/10.1306/03041312069

Bartholomew, I., Peters, J., & Powell, C. (1993). Regional structural evolution of the North Sea: Oblique slip and the reactivation of basement lineaments. *Geological Society, London, Petroleum Geology Conference Series*. Geological Society of London, 1109–1122.

Bell, R. E., Jackson, C. A. L., Whipp, P. S., & Clements, B. (2014). Strain migration during multiphase extension: Observations from the northern North Sea. *Tectonics*, *33*, 1936–1963. https://doi.org/10.1002/2014TC003551

Chopra, S., & Marfurt, K. J. (2007). *Seismic attributes for prospect identification and reservoir characterization (No. 11)*. Society of Exploration Geophysicists and European Association of Geoscientists and Engineers, SEG Books.

Clark, I. R., & Cartwright, J. A. (2009). Interactions between submarine channel systems and deformation in deepwater fold belts: Examples from the Levant Basin, Eastern Mediterranean sea. *Marine and Petroleum Geology*, *26*, 1465–1482.

Cook, A. E., & Sawyer, D. E. (2015). The mud-sand crossover on marine seismic data. *Geophysics*, *80*, A109–A114. https://doi.org/10.1190/geo2015-0291.1

Cowie, P., Gupta, S., & Dawers, N. (2000). Implications of fault array evolution for synrift depocentre development: Insights from a numerical fault growth model. *Basin Research*, *12*, 241–261.

Cowie, P. A., Underhill, J. R., Behn, M. D., Lin, J., & Gill, C. E. (2005). Spatio-temporal evolution of strain accumulation derived from multi-scale observations of Late Jurassic rifting in the northern North Sea: A critical test of models for lithospheric extension. *Earth and Planetary Science Letters*, *234*, 401–419.

Cullen, T. M., Collier, R. E. L., Gawthorpe, R. L., Hodgson, D. M., & Barrett, B. J. (2019). Axial and transverse deep-water sediment supply to syn-rift fault terraces: Insights from the West Xylokastro Fault Block, Gulf of Corinth, Greece. *Basin Research*, *32*, 1105–1139. https://doi.org/10.1111/bre.12416

Deptuck, M. E., Sylvester, Z., Pirmez, C., & O'Byrne, C. (2007). Migration–aggradation history and 3-D seismic geomorphology of submarine channels in the Pleistocene Benin-major Canyon, western Niger Delta slope. *Marine and Petroleum Geology*, *24*, 406–433.

Dreyer, T., Whitaker, M., Dexter, J., Flesche, H., & Larsen, E. (2005). From spit system to tide-dominated delta: Integrated reservoir model of the Upper Jurassic Sognefjord Formation on the Troll West Field. *Geological Society, London, Petroleum Geology Conference Series*. Geological Society of London, 423–448.

Duffy, O. B., Bell, R. E., Jackson, C.-A.-L., Gawthorpe, R. L., & Whipp, P. S. (2015). Fault growth and interactions in a multiphase rift fault network: Horda Platform, Norwegian North Sea. *Journal of Structural Geology*, *80*, 99–119.

Duffy, O., Brocklehurst, S., Gawthorpe, R., Leeder, M., & Finch, E. (2015). Controls on landscape and drainage evolution in regions of distributed normal faulting: Perachora Peninsula, Corinth Rift, Central Greece. *Basin Research*, *27*, 473–494. https://doi.org/10.1111/bre.12084

Ekdale, A. A., Bromley, R. G., & Knaust, D. (2012). The ichnofabric concept. *Developments in Sedimentology*, *64*, 139–155.

Færseth, R. (1996). Interaction of Permo-Triassic and Jurassic extensional fault-blocks during the development of the northern North Sea. *Journal of the Geological Society*, *153*, 931–944.

Færseth, R., Knudsen, B.-E., & Liljedahl, T. (1998). Oblique rifting and sequential faulting in the Jurassic development of the northern North Sea. *Oceanographic Literature Review*, *4*, 677.

Færseth, R. B., Knudsen, B. E., Liljedahl, T., Midbøe, P. S., & Søderstrøm, B. (1997). Oblique rifting and sequential faulting in the Jurassic development of the northern North Sea. *Journal of Structural Geology*, *19*, 1285–1302.

Færseth, R., & Ravnås, R. (1998). Evolution of the Oseberg fault-block in context of the northern North Sea structural framework. *Marine and Petroleum Geology*, *15*, 467–490.

Ford, M., Hemelsdaël, R., Mancini, M., & Palyvos, N. (2017). Rift migration and lateral propagation: Evolution of normal faults and sediment-routing systems of the western Corinth rift (Greece). *Geological Society, London, Special Publications*, *439*, 131–168. https://doi.org/10.1144/sp439.15

Fossen, H., Schultz, R. A., Rundhovde, E., Rotevatn, A., & Buckley, S. J. (2010). Fault linkage and graben stepovers in the Canyonlands (Utah) and the North Sea Viking Graben, with implications for hydrocarbon migration and accumulation. *AAPG Bulletin*, *94*, 597–613. https://doi.org/10.1306/10130909088

Fraser, S., Robinson, A., Johnson, H., Underhill, J., Kadolsky, D., Connell, R., Johannessen, P., & Ravnås, R. (2003). Upper Jurassic. In D. Evans, C. Graham, A. Armour & P. Bathurst (Eds.), *The Millennium atlas: Petroleum geology of the central and northern North Sea* (pp. 157–189). London: Geological Society.

Galloway, W. E. (1998). Siliciclastic slope and base-of-slope depositional systems: Component facies, stratigraphic architecture, and classification. *AAPG Bulletin-American Association of Petroleum Geologists*, *82*, 569–595.

Gawthorpe, R. L., Fraser, A. J., & Collier, R. E. L. (1994). Sequence stratigraphy in active extensional basins: Implications for the interpretation of ancient basin-fills. *Marine and Petroleum Geology*, *11*, 642–658.

Gawthorpe, R. L., & Leeder, M. R. (2000). Tectono-sedimentary evolution of active extensional basins. *Basin Research*, *12*, 195–218. https://doi.org/10.1046/j.1365-2117.2000.00121.x

Gawthorpe, R. L., Leeder, M. R., Kranis, H., Skourtsos, E., Andrews, J. E., Henstra, G. A., Mack, G. H., Muravchik, M., Turner, J. A., & Stamatakis, M. (2018). Tectono-sedimentary evolution of the Plio-Pleistocene Corinth rift, Greece. *Basin Research*, *30*, 448–479. https://doi.org/10.1111/bre.12260

Ge, Z., Nemec, W., Gawthorpe, R. L., & Hansen, E. W. M. (2017). Response of unconfined turbidity current to normal-fault topography. *Sedimentology*, *64*, 932–959. https://doi.org/10.1111/sed.12333

Ge, Z., Nemec, W., Gawthorpe, R. L., Rotevatn, A., & Hansen, E. W. M. (2017). Response of unconfined turbidity current to relay-ramp topography: Insights from process-based numerical modelling. *Basin Research*, *30*, 321–343. https://doi.org/10.1111/bre.12255

Glennie, K. (1990). Outline of North Sea history and structural framework. *Introduction to the Petroleum Geology of the North Sea*, *3*, 34–77.

Haughton, P. D., Barker, S. P., & McCaffrey, W. D. (2003). 'Linked' debrites in sand-rich turbidite systems–origin and significance. *Sedimentology*, *50*, 459–482.

Haughton, P., Davis, C., McCaffrey, W., & Barker, S. (2009). Hybrid sediment gravity flow deposits – Classification, origin and significance. *Marine and Petroleum Geology*, *26*, 1900–1918.

Henstra, G. A., Grundvåg, S.-A., Johannessen, E. P., Kristensen, T. B., Midtkandal, I., Nystuen, J. P., Rotevatn, A., Surlyk, F., Sæther, T., & Windelstad, J. (2016). Depositional processes and stratigraphic architecture within a coarse-grained rift-margin turbidite system: The Wollaston Forland Group, east Greenland. *Marine and Petroleum Geology*, *76*, 187–209.

Hizzett, J. L., Hughes Clarke, J. E., Sumner, E. J., Cartigny, M. J. B., Talling, P. J., & Clare, M. A. (2018). Which triggers produce the most erosive, frequent, and longest runout turbidity currents on deltas? *Geophysical Research Letters*, *45*, 855–863. https://doi.org/10.1002/2017gl075751

Holgate, N. E., Jackson, C.-A.-L., Hampson, G. J., & Dreyer, T. (2013). Sedimentology and sequence stratigraphy of the Middle-Upper Jurassic Krossfjord and Fensfjord formations, Troll Field, northern North Sea. *Petroleum Geoscience*, *19*, 237–258. https://doi.org/10.1144/petgeo2012-039

Holgate, N. E., Jackson, C. A., Hampson, G. J., & Dreyer, T. (2015). Seismic stratigraphic analysis of the Middle Jurassic Krossfjord and Fensfjord formations, Troll oil and gas field, northern North Sea. *Marine and Petroleum Geology*, *68*, 352–380.

Howlett, D. M., Ge, Z., Nemec, W., Gawthorpe, R. L., Rotevatn, A., & Jackson, C. A. L. (2019). Response of unconfined turbidity current to deep-water fold and thrust belt topography: Orthogonal incidence on solitary and segmented folds. *Sedimentology*, *66*, 2425–2454. https://doi.org/10.1111/sed.12602

Jackson, C. A. L., Barber, G. P., & Martinsen, O. J. (2008). Submarine slope morphology as a control on the development of sand-rich turbidite depositional systems: 3D seismic analysis of the Kyrre Fm (Upper Cretaceous), Måløy Slope, offshore Norway. *Marine and Petroleum Geology*, *25*, 663–680. https://doi.org/10.1016/j.marpetgeo.2007.12.007

Jackson, C. A. L., Gawthorpe, R. L., Leppard, C. W., & Sharp, I. R. (2006). Rift-initiation development of normal fault blocks: Insights from the Hammam Faraun fault block, Suez Rift, Egypt. *Journal of the Geological Society*, *163*, 165–183. https://doi.org/10.1144/0016-764904-164

Jackson, C.-A.-L., Larsen, E., Hanslien, S., & Tjemsland, A.-E. (2011). Controls on synrift turbidite deposition on the hanging wall of the South Viking Graben, North Sea rift system, offshore Norway. *AAPG Bulletin*, *95*, 1557–1587. https://doi.org/10.1306/01031110037

Jackson, C.-A.-L., McAndrew, A., Hodgson, D. M., & Dreyer, T. (2019). Repeated degradation and progradation of a submarine slope over geological timescales. *Earth Arxiv*. https://doi.org/10.31223/osf.io/6c2xv

Jackson, J., & Leeder, M. (1994). Drainage systems and the development of normal faults: An example from Pleasant Valley, Nevada. *Journal of Structural Geology*, *16*, 1041–1059. https://doi.org/10.1016/0191-8141(94)90051-5

Jia, J., Liu, Z., Miao, C., Fang, S., Zhou, R., Meng, Qi'an, Chen, Y., Yan, L., & Yang, D. I. (2014). Depositional model and evolution for a deep-water sublacustrine fan system from the syn-rift Lower

Cretaceous Nantun Formation of the Tanan Depression (Tamtsag Basin, Mongolia). *Marine and Petroleum Geology*, *57*, 264–282. https://doi.org/10.1016/j.marpetgeo.2014.05.022

Kane, I. A., Catterall, V., McCaffrey, W. D., & Martinsen, O. J. (2010). Submarine channel response to intrabasinal tectonics: The influence of lateral tilt. *AAPG Bulletin*, *94*, 189–219.

Kneller, B. C., Bennett, S. J., & McCaffrey, W. D. (1999). Velocity structure, turbulence and fluid stresses in experimental gravity currents. *Journal of Geophysical Research: Oceans*, *104*, 5381–5391. https://doi.org/10.1029/1998jc900077

Koch, J.-O., Frischbutter, A., Øygard, K., & Cater, J. (2017). The 35/9-7 Skarfjell discovery: A genuine stratigraphic trap, NE North Sea, Norway. *Geological Society, London, Petroleum Geology Conference Series*, *8*, 339–354. https://doi.org/10.1144/pgc8.34

Koson, S., Chenrai, P., & Choowong, M. (2014). Seismic attributes and their applications in seismic geomorphology. *Bulletin of Earth Sciences of Thailand*, *6*, 1–9.

Laake, A. (2015). Structural interpretation in color – A new RGB processing application for seismic data. *Interpretation*, *3*, SC1–SC8. https://doi.org/10.1190/int-2014-0041.1

Laughlin, K., Garossino, P., & Partyka, G. (2003). Spectral decomposition for seismic stratigraphic patterns: Search and Discovery. article 40096, 4p. http://www.searchanddiscovery.net/documents/geophysical/2003/laughlin/index.htm

Leeder, M. R., & Gawthorpe, R. L. (1987). Sedimentary models for extensional tilt-block/half-graben basins. *Geological Society, London, Special Publications*, *28*, 139–152. https://doi.org/10.1144/gsl.Sp.1987.028.01.11

Leppard, C. W., & Gawthorpe, R. L. (2006). Sedimentology of rift climax deep water systems; lower rudeis formation, hammam faraun fault block, Suez Rift, Egypt. *Sedimentary Geology*, *191*, 67–87.

Mayall, M., Jones, E., & Casey, M. (2006). Turbidite channel reservoirs – Key elements in facies prediction and effective development. *Marine and Petroleum Geology*, *23*, 821–841. https://doi.org/10.1016/j.marpetgeo.2006.08.001

McArdle, N., & Ackers, M. (2012). Understanding seismic thin-bed responses using frequency decomposition and RGB blending. *First Break*, *30*, 57–65.

McArthur, A. D., Hartley, A. J., Archer, S. G., Jolley, D. W., & Lawrence, H. M. (2016). Spatiotemporal relationships of deep-marine, axial, and transverse depositional systems from the synrift Upper Jurassic of the central North Sea. *AAPG Bulletin*, *100*, 1469–1500. https://doi.org/10.1306/04041615125

McHargue, T., Pyrcz, M. J., Sullivan, M. D., Clark, J., Fildani, A., Romans, B., Covault, J., Levy, M., Posamentier, H. W., & Drinkwater, N. J. (2011). Architecture of turbidite channel systems on the continental slope: Patterns and predictions. *Marine and Petroleum Geology*, *28*, 728–743.

Muravchik, M., Gawthorpe, R. L., Sharp, I. R., Rarity, F., & Hodgetts, D. (2018). Sedimentary environment evolution in a marine hanging-wall dipslope setting. El Qaa Fault Block, Suez Rift, Egypt. *Basin Research*, *30*, 452–478. https://doi.org/10.1111/bre.12231

Muravchik, M., Henstra, G. A., Eliassen, G. T., Gawthorpe, R. L., Leeder, M., Kranis, H., Skourtsos, E., & Andrews, J. (2019). Deep-water sediment transport patterns and basin floor topography in early rift basins: Plio-Pleistocene syn-rift of the Corinth Rift, Greece. *Basin Research*, *32*, 1184–1212. https://doi.org/10.1111/bre.12423

Muto, T., & Steel, R. (2002). In defense of shelf-edge delta development during falling and lowstand of relative sea level. *The Journal of Geology*, *110*, 421–436. https://doi.org/10.1086/340631

Nelson, H. C., Karabanov, E. B., Colman, S. M., & Escutia, C. (1999). Tectonic and sediment supply control of deep rift lake turbidite systems: Lake Baikal, Russia. *Geology*, *27*, 163–166. https://doi.org/10.1130/0091-7613(1999)027<0163:Tassco>2.3.Co;2

Nøttvedt, A., Berge, A. M., Dawers, N. H., Færseth, R. B., Häger, K. O., Mangerud, G., & Puigdefabregas, C. (2000). Syn-rift evolution and resulting play models in the Snorre-H area, northern North Sea. *Geological Society, London, Special Publications*, *167*, 179–218. https://doi.org/10.1144/gsl.Sp.2000.167.01.08

Odinsen, T., Reemst, P., Van Der Beek, P., Faleide, J. I., & Gabrielsen, R. H. (2000). Permo-Triassic and Jurassic extension in the northern North Sea: Results from tectonostratigraphic forward modelling. *Geological Society, London, Special Publications*, *167*, 83–103.

Partington, M., Copestake, P., Mitchener, B. A., & Underhill, J. R. (1993). Biostratigraphic calibration of genetic stratigraphic sequences in the Jurassic–lowermost Cretaceous (Hettangian to Ryazanian) of the North Sea and adjacent areas. *Geological Society, London, Petroleum Geology Conference Series*. Geological Society of London, 371–386.

Partington, M., Mitchener, B., Milton, N., & Fraser, A. (1993). Genetic sequence stratigraphy for the North Sea Late Jurassic and Early Cretaceous: Distribution and prediction of Kimmeridgian-Late Ryazanian reservoirs in the North Sea and adjacent areas. *Geological Society, London, Petroleum Geology Conference Series*. Geological Society of London, 347–370.

Partyka, G., Gridley, J., & Lopez, J. (1999). Interpretational applications of spectral decomposition in reservoir characterization. *The Leading Edge*, *18*, 353–360.

Patruno, S., Hampson, G. J., Jackson, C.-A.-L., & Dreyer, T. (2015). Clinoform geometry, geomorphology, facies character and stratigraphic architecture of a sand-rich subaqueous delta: Jurassic Sognefjord Formation, offshore Norway. *Sedimentology*, *62*, 350–388. https://doi.org/10.1111/sed.12153

Phillips, T., Fazlikhani, H., Gawthorpe, R., Fossen, H., Jackson, C.-A.-L., Bell, R., Faleide, J. I., & Rotevatn, A. (2019). The influence of structural inheritance and multiphase extension on rift development, the northern North Sea. *Tectonics*, *38*, 4099–4126. https://doi.org/10.1029/2019TC005756

Piper, D. J. W., & Normark, W. R. (2009). Processes that initiate turbidity currents and their influence on turbidites: A marine geology perspective. *Journal of Sedimentary Research*, *79*, 347–362. https://doi.org/10.2110/jsr.2009.046

Pivnik, D. A., Ramzy, M., Steer, B. L., Thorseth, J., El Sisi, Z., Gaafar, I., Garing, J. D., & Tucker, R. S. (2003). Episodic growth of normal faults as recorded by syntectonic sediments, July oil field, Suez rift, Egypt. *AAPG Bulletin*, *87*, 1015–1030. https://doi.org/10.1306/02050301100

Plink-Björklund, P., & Steel, R. J. (2004). Initiation of turbidity currents: Outcrop evidence for Eocene hyperpycnal flow turbidites. *Sedimentary Geology*, *165*, 29–52.

Posamentier, H. W., & Kolla, V. (2003). Seismic geomorphology and stratigraphy of depositional elements in deep-water settings. *Journal of Sedimentary Research*, *73*, 367–388. https://doi.org/10.1306/111302730367

Prather, B. E. (2003). Controls on reservoir distribution, architecture and stratigraphic trapping in slope settings. *Marine and Petroleum Geology*, *20*, 529–545. https://doi.org/10.1016/j.marpetgeo.2003.03.009

Prather, B. E., Booth, J. R., Steffens, G. S., & Craig, P. A. (1998). Classification, lithologic calibration, and stratigraphic succession

of seismic facies of intraslope basins, deep-water Gulf of Mexico. *AAPG Bulletin*, *82*, 701–728.

Prélat, A., Hodgson, D. M., & Flint, S. S. (2009). Evolution, architecture and hierarchy of distributary deep-water deposits: A high-resolution outcrop investigation from the Permian Karoo Basin, South Africa. *Sedimentology*, *56*, 2132–2154. https://doi.org/10.1111/j.1365-3091.2009.01073.x

Prosser, S. (1993). Rift-related linked depositional systems and their seismic expression. *Geological Society, London, Special Publications*, *71*, 35–66. https://doi.org/10.1144/gsl.Sp.1993.071.01.03

Ravnås, R., & Bondevik, K. (1997). Architecture and controls on Bathonian-Kimmeridgian shallow-marine synrift wedges of the Oseberg-Brage area, northern North Sea. *Basin Research*, *9*, 197–226.

Ravnås, R., Nøttvedt, A., Steel, R. J., & Windelstad, J. (2000). Syn-rift sedimentary architectures in the Northern North Sea. *Geological Society, London, Special Publications*, *167*, 133–177. https://doi.org/10.1144/gsl.sp.2000.167.01.07

Ravnås, R., & Steel, R. J. (1997). Contrasting styles of Late Jurassic syn-rift turbidite sedimentation: A comparative study of the Magnus and Oseberg areas, northern North Sea. *Marine and Petroleum Geology*, *14*, 417–449.

Ravnås, R., & Steel, R. (1998). Architecture of marine rift-basin successions. *AAPG Bulletin*, *82*, 110–146.

Reading, H. G., & Richards, M. (1994). Turbidite systems in deep-water basin margins classified by grain size and feeder system. *AAPG Bulletin*, *78*, 792–822. https://doi.org/10.1306/a25fe3bf-171b-11d7-8645000102c1865d

Reeve, M. T., Bell, R. E., Duffy, O. B., Jackson, C.-A.-L., & Sansom, E. (2015). The growth of non-colinear normal fault systems; What can we learn from 3D seismic reflection data? *Journal of Structural Geology*, *70*, 141–155.

Richards, M., Bowman, M., & Reading, H. (1998). Submarine-fan systems i: Characterization and stratigraphic prediction. *Marine and Petroleum Geology*, *15*, 689–717. https://doi.org/10.1016/s0264-8172(98)00036-1

Roberts, A. M., Kusznir, N. J., Yielding, G., & Beeley, H. (2019). Mapping the bathymetric evolution of the Northern North Sea: From Jurassic synrift archipelago through Cretaceous-Tertiary post-rift subsidence. *Petroleum Geoscience*, *25*, 306–321. https://doi.org/10.1144/petgeo2018-066

Saller, A., Werner, K., Sugiaman, F., Cebastiant, A., May, R., Glenn, D., & Barker, C. (2008). Characteristics of Pleistocene deep-water fan lobes and their application to an upper Miocene reservoir model, offshore East Kalimantan, Indonesia. *AAPG Bulletin*, *92*, 919–949. https://doi.org/10.1306/03310807110

Scholz, C. A., Rosendahl, B. R., & Scott, D. L. (1990). Development of coarse-grained facies in lacustrine rift basins: Examples from East Africa. *Geology*, *18*, 140–144. https://doi.org/10.1130/0091-7613(1990)018<0140:Docgfi>2.3.Co;2

Shultz, M. R., & Hubbard, S. M. (2005). Sedimentology, stratigraphic architecture, and ichnology of gravity-flow deposits partially ponded in a growth-fault-controlled slope minibasin, Tres Pasos Formation (Cretaceous), southern Chile. *Journal of Sedimentary Research*, *75*, 440–453. https://doi.org/10.2110/jsr.2005.034

Sømme, T. O., & Jackson, C. A. L. (2013). Source-to-sink analysis of ancient sedimentary systems using a subsurface case study from the Møre-Trøndelag area of southern Norway: Part 2 – Sediment dispersal and forcing mechanisms. *Basin Research*, *25*, 512–531. https://doi.org/10.1111/bre.12014

Sømme, T. O., Jackson, C. A. L., & Vaksdal, M. (2013). Source-to-sink analysis of ancient sedimentary systems using a subsurface case study from the Møre-Trøndelag area of southern Norway: Part 1 – Depositional setting and fan evolution. *Basin Research*, *25*, 489–511. https://doi.org/10.1111/bre.12013

Stewart, D., Schwander, M., & Bolle, L. (1995). Jurassic depositional systems of the Horda Platform, Norwegian North Sea: Practical consequences of applying sequence stratigraphic models. *Norwegian Petroleum Society Special Publications*, *5*, 291–323.

Stow, D. A., & Mayall, M. (2000). Deep-water sedimentary systems: New models for the 21st century. *Marine and Petroleum Geology*, *17*, 125–135.

Turner, C., Cronin, B., Riley, L., Patruno, S., Reid, W., Hoth, S., Knaust, D., Allerton, S., Jones, M. A., & Jackson, C.-A.-L. (2018). The South Viking 1 Graben: Overview of Upper Jurassic rift geometry, biostratigraphy and extent of Brae Play submarine fan systems. In C. Turner & B. T. Cronin. (Eds.), *Riftrelated coarse-grained submarine fan reservoirs; the Brae Play, South Viking Graben, North Sea*, American Association of Petroleum Geologists, Memoirs, 115.

Vollset, J., & Doré, A. G. (1984). *A revised Triassic and Jurassic lithostratigraphic nomenclature for the Norwegian North Sea*. Oljedirektoratet.

Whipp, P., Jackson, C., Gawthorpe, R., Dreyer, T., & Quinn, D. (2014). Normal fault array evolution above a reactivated rift fabric; a subsurface example from the northern Horda Platform, Norwegian North Sea. *Basin Research*, *26*, 523–549. https://doi.org/10.1111/bre.12050

Younes, A. I., & McClay, K. (2002). Development of accommodation zones in the Gulf of Suez-Red Sea Rift, Egypt. *AAPG Bulletin*, *86*, 1003–1026. https://doi.org/10.1306/61eedc10-173e-11d7-8645000102c1865d

Zanella, E., Coward, M., Evans, D., Graham, C., Armour, A., & Bathurst, P. (2003). Structural framework. In D. Evans, C. Graham, A. Armour & P. Bathurst. (Eds.), *The Millennium atlas: Petroleum geology of the central and northern North Sea* (pp. 45–59). London: Geological Society.

Zhang, X., & Scholz, C. A. (2015). Turbidite systems of lacustrine rift basins: Examples from the Lake Kivu and Lake Albert rifts, East Africa. *Sedimentary Geology*, *325*, 177–191. https://doi.org/10.1016/j.sedgeo.2015.06.003

Zhang, X., Scholz, C. A., Hecky, R. E., Wood, D. A., Zal, H. J., & Ebinger, C. J. (2014). Climatic control of the late Quaternary turbidite sedimentology of Lake Kivu, East Africa: Implications for deep mixing and geologic hazards. *Geology*, *42*, 811–814. https://doi.org/10.1130/g35818.1

Zhong, X., Escalona, A., & Augustsson, C. (2020). Architecture of shoreface to deep-water systems in segmented rift systems: Evidence from the southern margin of the Sogn Graben, northern North Sea. *Marine and Petroleum Geology*, *117*, 104361. https://doi.org/10.1016/j.marpetgeo.2020.104361

How to cite this article: Tillmans F, Gawthorpe RL, Jackson CA-L, Rotevatn A. Syn-rift sediment gravity flow deposition on a Late Jurassic fault-terraced slope, northern North Sea. *Basin Res*. 2021;33:1844–1879. https://doi.org/10.1111/bre.12538